Virginia Tech Morphing Wing Team Fall 2004 Final Report

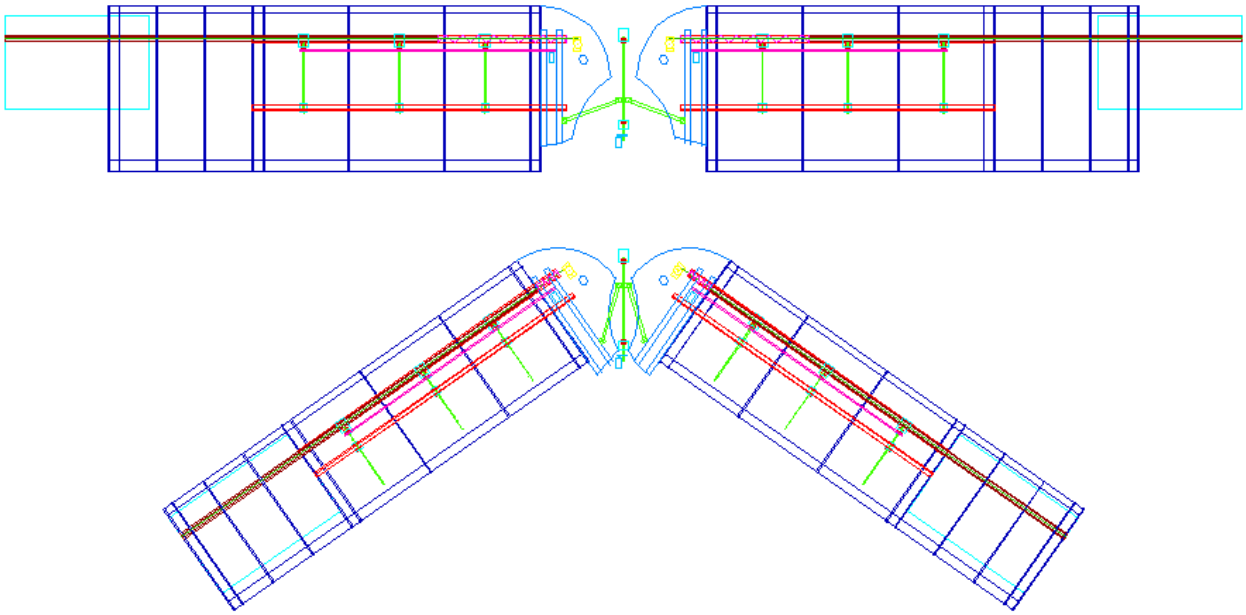

Desta Alemayehu
Mathieu Leng
Ryan McNulty
Michael Mulloy
Ryan Somero
Cyril de Tenorio
Aerospace and Mechanical Engineering Departments
Virginia Tech
December 16, 2004

Table of Contents

1.0 Introduction

It has always been the goal of aerospace engineers to design planes that fly faster, further, and higher. With today's technology we are able to fly faster than ten times the speed of sound, around the world without refueling, and over 350,000 feet high, but none of these planes could do all three. With every design come tradeoffs between the different flight regimes. Traditional fixed wing geometry aircraft are designed to efficiently fly within one flight regime. Morphing wing technology, however, has begun to break down the barriers of tradeoffs.

2.0 Background

2.1 History of Morphing Technology

On June 10, 1951, the X-5 by Bell Aircraft became the world's first aircraft to sweep back its wings during flight. The X-5 was built to demonstrate the ability to sweep in flight angles of 20,45, and 60 degrees at subsonic and transonic speeds. The X-5's ability to successfully demonstrate this capability made way for the first military use of swept wings with Grumman Aircraft's F-10-F. Refer to figure 1 for an image of the Grumman F-10-F.

Figure 1. Image of Grumman F-10-F. The F-10-F was one of the first airplanes to have a morphing wing geometry [pilotfriend.com, 2004].

The United States Navy today takes advantage of the ability to change the sweep angle with the F-14 Tomcat. The F-14's normal sweep range is from 20 to 68 degrees and is able to "over sweep" to 75 degrees. The slightly swept wing position is ideal of short take off and landings from carriers, as well as low speed and fuel-efficient flight. The fully swept back position is ideal for supersonic speeds, maneuverability, and aircraft storage on the carrier. The ability to morph gives the F-14 the ability to fly at speeds up to Mach 1.88 and up to a range of 500 nautical miles. Figure 2 shows three different perspectives of the F-14.

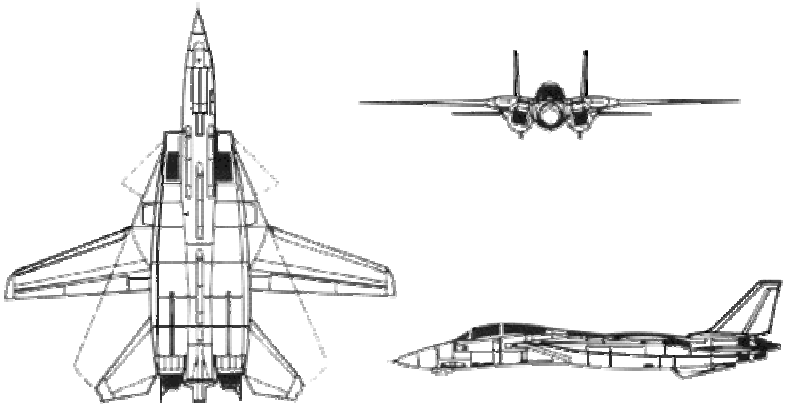

Figure 2. Top, front, and side view of F-14 tomcat. The F-14 has the ability to sweep up to 68 degrees in flight [fas.org, 2004].

2.2 Morphing Aircraft of the Future

The Defense Advanced Research Projects Agency, DARPA, is working to develop an aircraft with the ability to morph in a far more dramatic fashion than currently possible. Lockheed Martin and NexGen Aeronautics have both developed an initial prototype for this project. Lockheed Martin's concept involves a folding wing technology, similar to that of a sea gull's wings. The wings fold up to the fuselage and are deployed for the full span condition. Figure 3 shows a picture of Lockheed Martin's concept. NexGen's concept uses a sliding skin technology. The use of sliding skin allows for sweep, chord, and span change without the heavy pin joints required with today's variable sweep fighters. Using the sliding skin technology, the air loads are distributed over a greater area, decreasing the necessary strength of joints and therefore decreasing

the weight of those joints. The NexGen Concept is capable of optimizing performance for high speed flight, take off and landing, maneuvering, and loitering. Figure 4 shows an image of NexGen's morphing wing design.

Figure 3. Image of Lockheed Martin's morphing wing design. This plane does not implement a stretching skin design, it have wing sections that fold up [NewScientist.com, 2003].

Figure 4. Image of NexGen's morphing wing concept. This design requires a stretching skin to allow the wing to morph [NewScientist.com, 2003].

2.3 2004 Morphing Wing Team Goals

It is the goal of the 2004 Virginia Tech Morphing Wing team to develop and build a morphing wing capable of optimizing its performance in four flight regimes: Dash, Maneuvering, Loiter, and Take-off / Landing.

The Dash regime is defined as a high-speed attack regime. It is configured for a low surface area, low span, and high sweep angle. This configuration produces low drag by having a streamlined profile as well as low induced drag.

The Loiter regime is defined for high endurance. It is configured to have a high aspect ratio and low sweep angle. The Loiter regime is designed to perform at minimum power and low speeds to allow for maximum time in the air.

The Maneuvering regime is defined as a maximum control regime. It is configured for high lift capability and late and controlled stall. This regime experiences high structural loads due to the high load maneuvers.

3.0 Design Process

The following section discusses the design process used to build the full scale morphing wing wind tunnel model. The section begins with a description of each actuation concept and follows with the final actuation selection. The section then discusses the electrical system design and its components. Finally, the section ends with the design of support equipment used to test the full scale model in the wind tunnel.

3.1 Actuation Design Possibilities

Sweep As stated earlier the goal for this project is to have the wing shape morph three different ways: sweep change, span change, and changing of the chord length. For the sweep change we first came up with how much of an angle we wanted the wing to arc back to. The team came up with a goal of sweeping approximately 30-40 degrees. The first idea for implementing this was one design named the rotating beams. This idea was generated first to perform a change in chord length but had the added bonus of also allowing for a change in the sweep angle. The idea consisted of two separate airfoil structures that are connected in the middle by rods in a diamond configuration. These rods would be hinged at each end so that they can swivel or rotate. This is almost the same idea a car jack uses. Pulling the two ends of the diamond in will separate or push the other ends apart. Since there is an open space in between the two airfoil sections where the rods will be placed, a skirt would be needed to fill this gap in order to keep a smooth airfoil shape. Figure 5 shows the rotating beam design and how the rods are configured in a diamond shape. With this design there is a need for the back spar to have the ability to slide along a track. By allowing both the front and back spar to swivel, the design now allows for a change in sweep angle.

Figure 5. Model of rotating beam design. Notice diamond rod structures allow for both sweep and chord change.

This design is advantageous for our team because of the simplicity for having two different airfoil sections. Two different airfoil sections would be easier to construct for the chord change aspect instead of having to mesh two separate ribs. The diamond rods will also add a strong structure to the wing so heavier loads can be supported.

Although this design had many advantages, it would not allow our team to meet all the goals of this project. With the diamond rods that actuated the wing for chord length change and a change in sweep angle, there would be no room for the span extension in the wing. With this design only two out of the three changes could occur.

The next competing idea for the sweep change was a gear turntable. The design called for a turntable for which all of the chord change and span change actuation components would be placed on. The turntable would be arched on the side opposite of the wing and would have a geared track along the arch. A motor with a gear on it would be stationary in the fuselage and would run along the geared track. The turntable would rotate around a pin that would be attached to the fuselage with bearings. Please refer to Figure 6 for a drawing of the geared turntable.

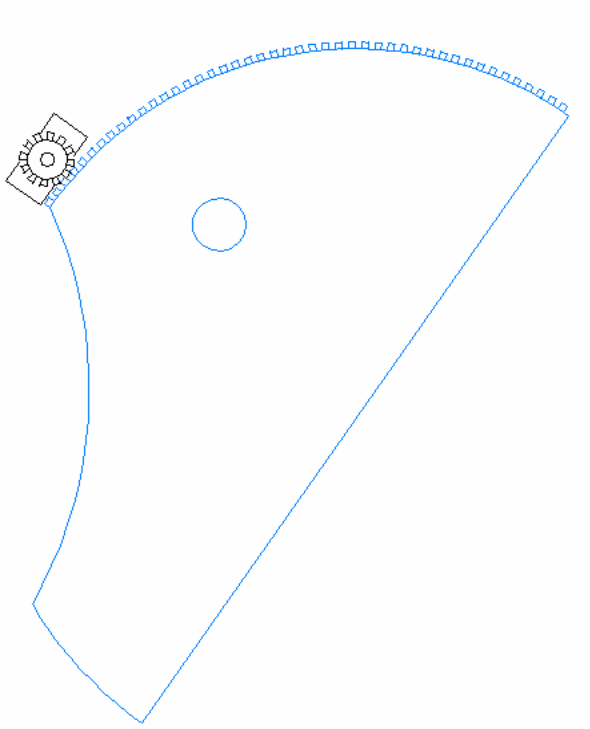

Figure 6. AutoCAD drawing of geared turntable. As motor rotates clockwise the turntable rotates counterclockwise.

This design allowed for any amount of sweep our team wanted to get for our design. It also was pretty simple to implement while also housing most actuation in a compact area. The main problem with this design is where the loading will concentrate and what component will take the load. During flight the wing will have to withstand air trying to push it back since it is able to pivot. With this geared track design the only component that is preventing this wing from folding back is the motor. This load concentration will cause the sweep actuation to become difficult and could also damage the motor. A worse-case scenario could also be one wing giving way and folding back while the other does not, causing a catastrophic failure of the airplane. Our team ended up not wanting to put such a load concentration on a weak component such as the motor.

The final design was very similar to the geared track method with one slight difference. The turntable is still used in this design, except the actuation of the turntable has changed. Now, in order to eliminate the load concentration on the motor, a power screw is used to drive the turntable. A motor drives a stationary power screw that has a threaded block attached to it. Depending on the direction the motor is turning this threaded block will travel the length of the power screw. The threaded block has push rods attached to it which are also connected to the

turntable. When the block moves along the power screw the turntable rotates one way or another, causing a change in sweep angle. Figure 7 shows how the geared track is now replaced with a power screw.

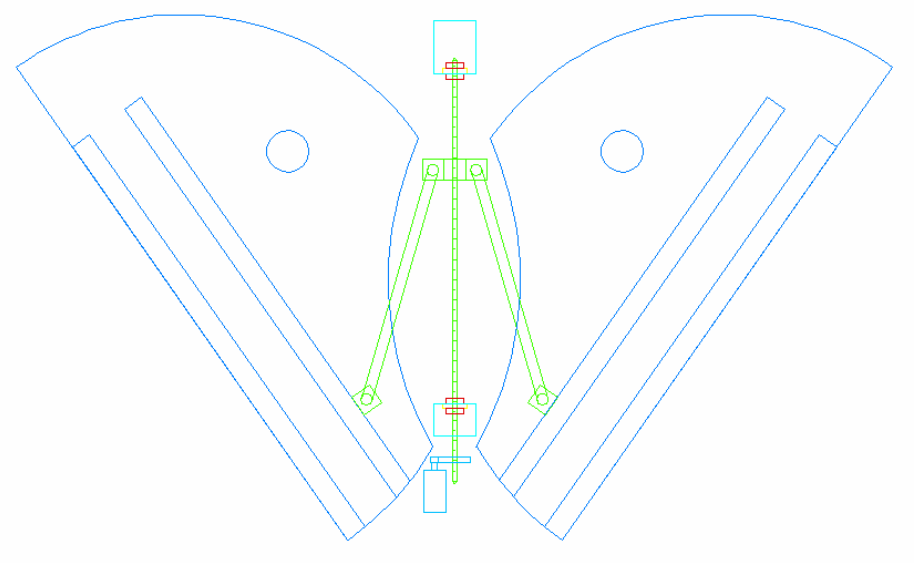

Figure 7. AutoCAD drawing of power screw turntable. The threaded sweep block travels up and down the power screw to sweep the wings forward or back.

This design eliminates the load concentration on the motor and moves it to a more sturdy power screw. The design also slows the speed at which the change happens. Since motors spin at a high RPM, a geared track design would move very quickly and could even cause problems such as stripping gears due to such a high speed. Now that a power screw is used, the gear ratio between the motor sprocket and the threads of the screw, the rotation is brought to a more reasonable speed.

Chord The airfoil shape of a wing is created by arced structural members called ribs. These components make it difficult to perform a change in the chord length of a wing. The hardest part of this actuation is finding some sort of stretching skin to cover the wing with. This stretching skin would be needed so as the ribs expand the airfoil shape of the wing is still preserved. To overcome this challenge we came up with three different designs which consist of two different solid airfoil sections that eliminate the need for a stretching skin.

The first concept is what was used also for one of the sweep designs. The rotating beams concept has the diamond shaped structures which are able to contract and expand based on movement of the back spar. The back spar would have had a geared track that would be attached to a motor and sprocket. When the motor was turned on the back spar would travel forward or

backward, creating a change in chord length. Please refer back to figure 1 for a picture of the diamond rod structures.

A problem with this design is that, as stated before, there would be the need for a skirt to cover the area in between the two separate airfoil sections to cover the diamond structures. Aerodynamic forces on this skirt could cause it to separate from the wing, loosing the airfoil shape. Once again, the major downfall of this design is it would not be able to accommodate room for an extension for span change.

The next design involves three ribs attached together to slide past each other. As you can see in Figure 8, each single rib of a normal wing is replaced by three separate half ribs. These ribs are connected by a track in the middle of each of them. With a screw running inside the track, the ribs are able to slide back and forth which causes a change in chord length. The front and back sections are also separately covered by monokote so a stretching skin is not needed. This design was going to be actuated by a set of power screws attached to the main spar that would be powered by a motor and chain system. A motor would turn a chain that is attached to the power screws, which in turn will cause a threaded back spar to travel up or down the power screws. Figure 9 shows a picture of how this process would be implemented.

Figure 8. Model of sliding rib design. A skirt is needed to cover the gap when the chord is extended.

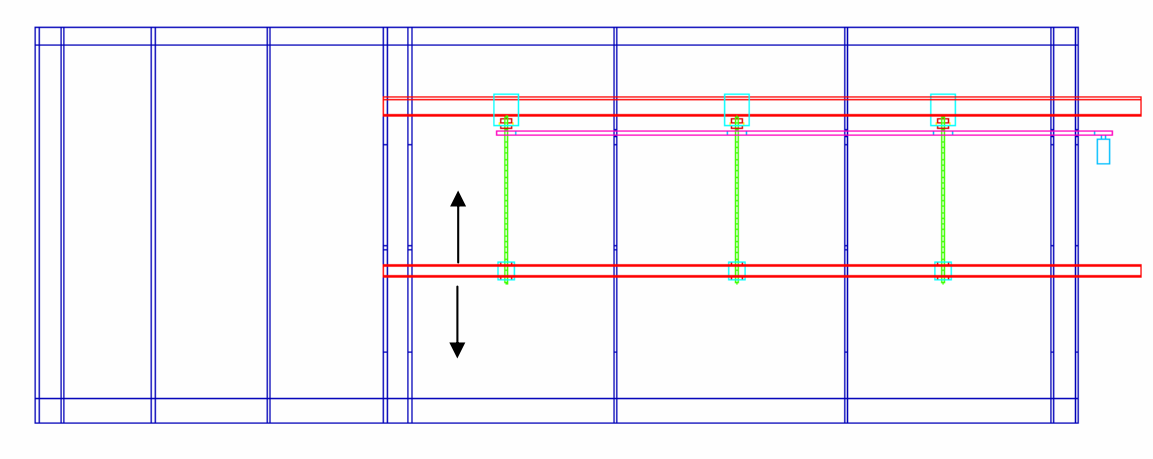

Figure 9. AutoCAD drawing of chord change using power screws. Lower spar travels up and down the power screw changing chord length.

Similar to the rotating beam design, this also requires a skirt to cover the two sections so that a smooth airfoil shape is kept. As stated before, this causes the problem of aerodynamic forces lifting up the skirt, changing the airfoil shape. Although this design does require the need for a skirt, this concept does allow for there to be a change in span.

The final concept that was developed is the C-socket design. This concept takes the best ideas from the previous two concepts. This design is best described as two separate airfoil sections that are powered by a series of power screws with a threaded back spar. Eliminating the diamond structure and replacing it with the power screws we are able to make room for a span extension. With these diamond structures gone we are also able to move the two airfoil sections closer together so that a skirt between the two is no longer needed. Figure 10 illustrates the basic concept of the C-socket design.

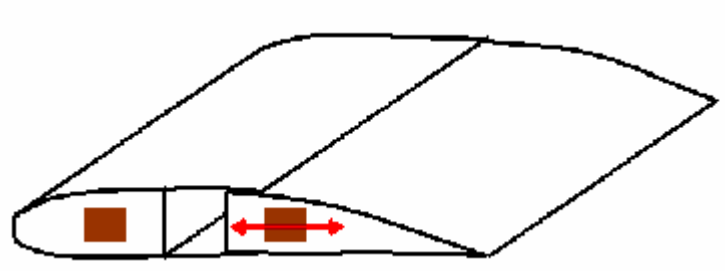

Figure 10. Diagram of C-socket chord design. This design does not require a skirt.

This design basically eliminates almost all of the problems the other two concepts had. With it our team is able to meet all 3 morphing changes we are aiming for, while at the same time found

a plausible and relatively easy design to implement. This also has fewer components in the wing, making this design lighter than the other two.

Span For the implementation of the span change, only one main idea was thought up. The idea was developed and our whole team liked it so we decided it would work the best. The only aspect that was debated and had to be decided on was how to implement the idea. The basic concept was to have a smaller wing inside the main wing body that would be pushed out by the smaller wings spar. The smaller spar, which was made of carbon fiber, would travel in and out of a hollow carbon fiber main wing spar. Figure 11 shows the basic concept of the main wing housing a smaller wing. The first idea was to have a geared track attached to the smaller wings spar which would be moved by a motor inside of the fuselage. The problem with this concept is that once fully contracted, the smaller wings spar would need room inside of the fuselage otherwise it would be sticking out of the other side.

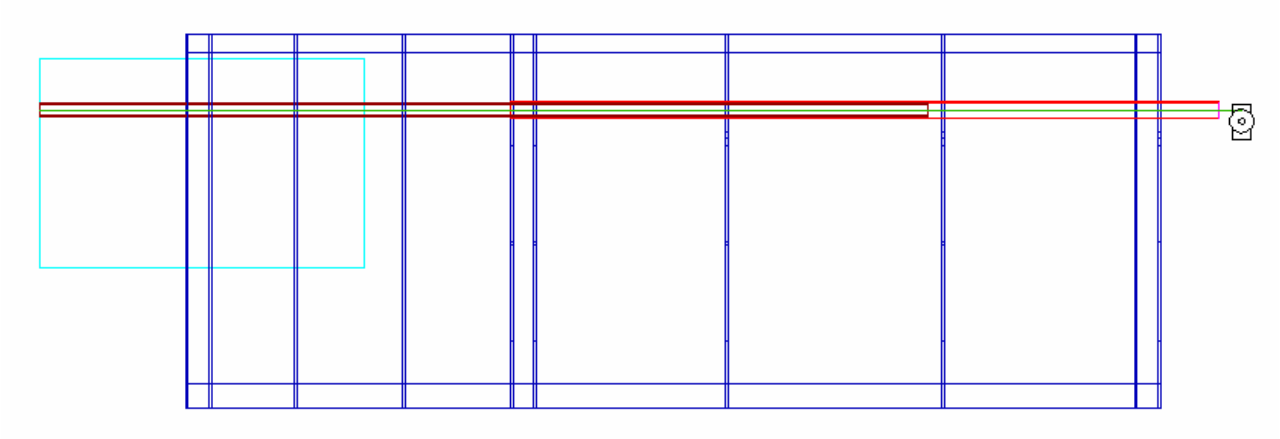

Figure 11. AutoCAD drawing of span extension. This drawing shows the span only half extended.

The next idea which was thought up to overcome the last concepts problem was use of a winch servo. A winch servo can rotate approximately three times each direction. Using a fifty pound test fishing line, the servo head would be counter wrapped. When the servo spins in one direction one line will unwind while the other wraps up. Using this concept the spar of the small extension can be pulled in either direction: out of the wing, or in. This design eliminated the need for housing the spar when fully contracted and also aloud for use of a servo which can easily be operated using a receiver and remote control. The downfall of this design is that the winch servo to be used requires a 7.2volt 1500mA 6 cell NiCad battery; which is a relatively heavy battery.

3.2 Actuation Design Decisions

After discussing the three different concepts to actuate the sweep, the power screw operated turntable was the team's final decision. This design removed the load concentration from the motor used for actuation and also geared down the motor. This would not cause the sweeping to occur at such a fast speed.

The chord change was decided on based on which design would be the lightest while also being able to complete all three of our mission goals. The C-socket design left room in the wing for housing of the span extension while also having the lightest actuation weight inside of the wing, so this was the design chosen.

The components used for a change in span were easily decided to be a smaller wing shape housed inside the main wing. But the harder decision was which way to actuate this small wing. After considering the amount of room each design would take up once contracted, the winch servo pull-pull system proved to be the better choice.

3.3 Electrical Design

Each mechanical component of the design also required an electrical sub-system to drive its moving parts. The sweep actuation relied on the rotation of the main power screw within the fuselage to sweep the wings forward and back. To turn the threaded rod we decided on a lightweight DC motor like the one shown in Figure 12. To stop the sweep block from traveling too far up or down the power screw we also needed a pair of kill switches like the one shown in Figure 13.

Figure 12. Image of DC electric motor [radioshack.com, 2004]. This motor is rated from 9 to 18 V.

Figure 13. Image of kill switch [radioshack.com, 2004]. Two kill switches limit the forward and reverse travel of the sweep block.

To allow the motor to start and stop and go from forward to reverse we used a three-point toggle switch like the one shown in Figure 14. In the center position no current is allowed to pass through the switch. Shifting the switch to either side results in a polarity change and engages the motor. To control the motor speed we connected a potentiometer, like the ones shown in Figure 15, in parallel with the motor terminals. By limiting the voltage across the motor we can increase and decrease its rotational speed. Adding these speed controllers allowed the team to adjust the actuation rate on-site.

Figure 14. Image of center-off toggle switch [radioshack.com, 2004]. The center position supplies no power to the motor while the left and right positions correspond to forward and reverse.

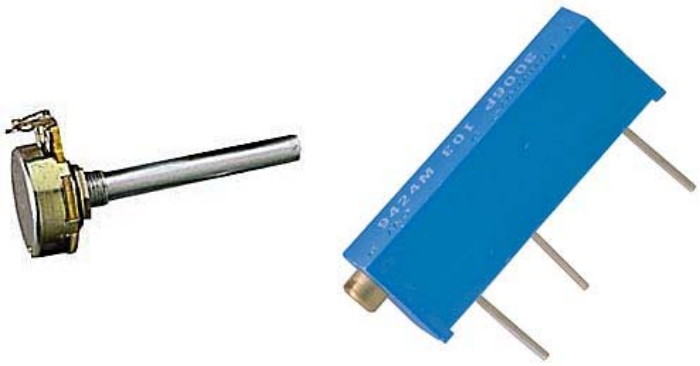

Figure 15. Images of two types of potentiometers [radioshack.com, 2004]. By rotating the shafts in the potentiometers the resistance is varied.

Figure 16 is a diagram of the electrical system used for the sweep actuation. The circuit is powered by two 9 V alkaline batteries and is controlled with the toggle switch. When the switch is thrown forward the motor rotates the shaft through a pinion/spur gear system until the sweep block trips the first kill switch. The kill switch cuts the power to the motor which causes it to stop. This position corresponds to the wings being swept back to their maximum angle. When the toggle switch is moved to the reverse position the second circuit becomes active and the polarity is reversed across the motor. The motor then rotates in reverse until the second kill switch is tripped. This position is back to a sweep angle of zero.

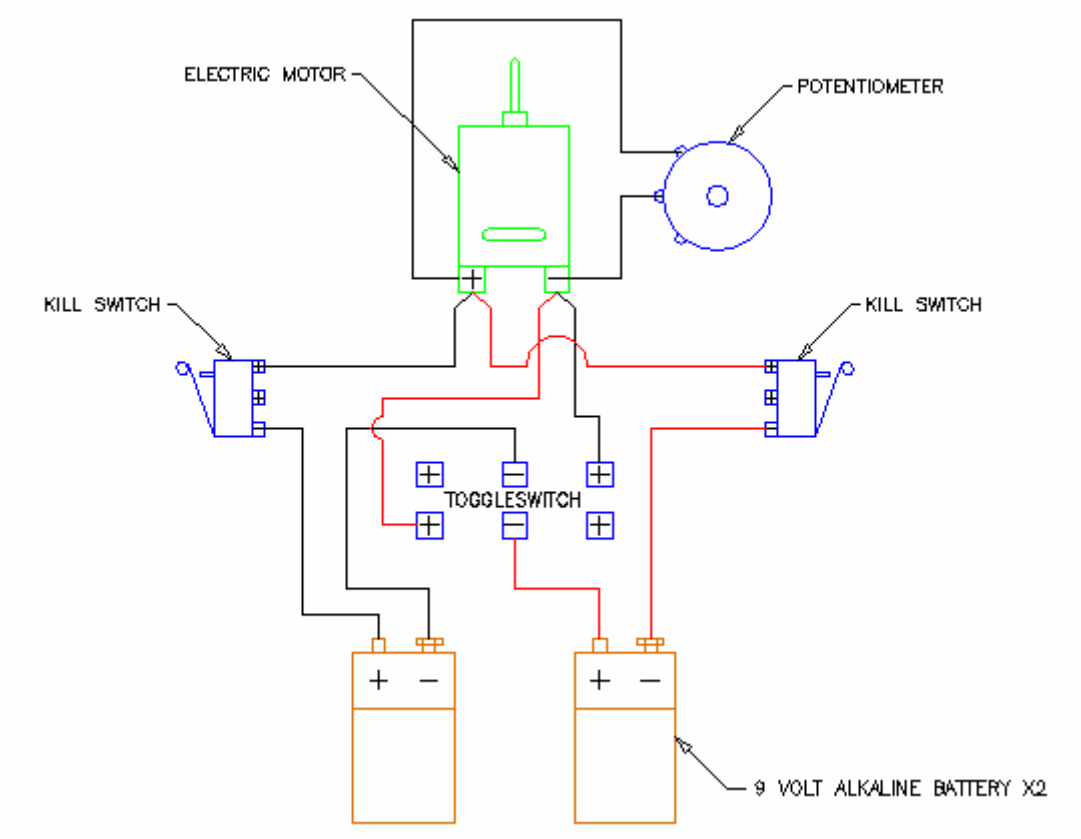

Figure 16. Circuit diagram used in sweep and chord actuation. The toggle switch alternates between the forward and reverse circuits.

The same setup for the sweep was also used for the chord actuation. As the motor rotates in the forward position the chord mechanism extends and when the motor rotates in reverse the chord retracts. The only difference is that the motor now has a sprocket fixed to its shaft and turns a plastic chain. Figure 17 is an image of the mock up we used to test the sweep/chord circuit. The test system certified that our design was indeed viable.

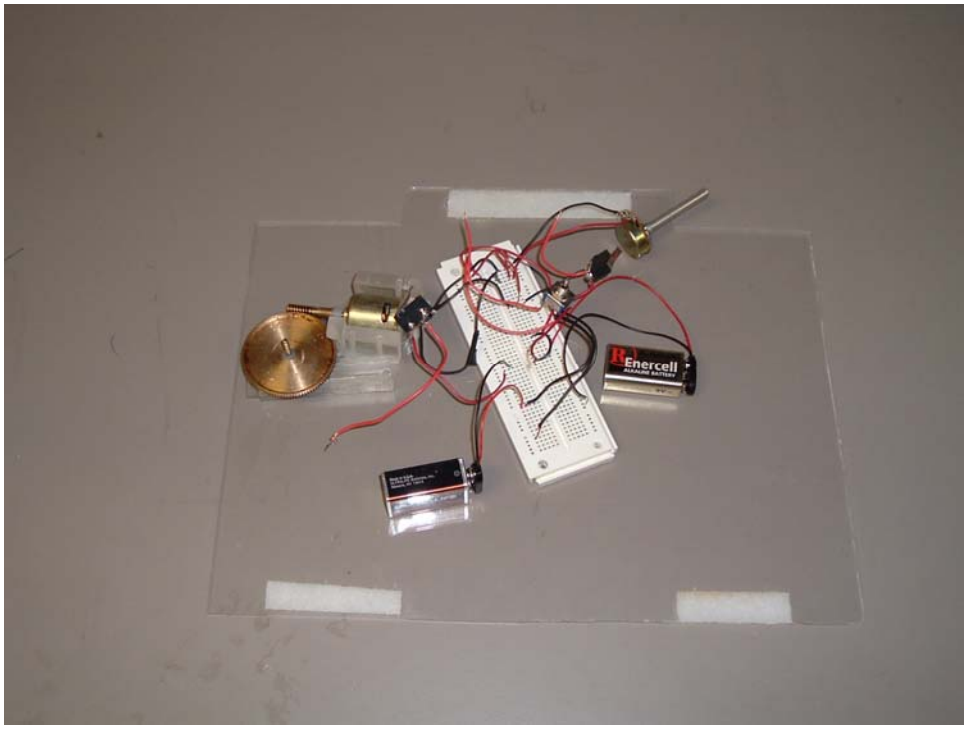

Figure 17. Test setup for sweep/chord electrical system. This test setup was made of spare parts and was not the one included in the full wing model.

To actuate the span change we decided to use the Futaba winch servo shown in Figure 18. The servo has an individual on and off switch and is powered by a 7.2 V battery pack. The drum can make six total revolutions and has a torque rating of up to 136 oz-in. The servo is connected directly into the receiver and requires no additional wiring.

Figure 18. Futaba sail winch servo [towerhobbies.com, 2004]. The winch servo is powered by a 6-cell, 7.2 V, Ni-Cd battery pack.

3.4 Wind Tunnel Equipment Design

The Virginia Tech wind tunnel, as shown in Figure 19, has a cross-section that is 6’ x 6’. Since the instrumentation strut is over 3’ tall we needed to design our own mount to test the 4’. - 4” full sized wing model. The model needs to bolt to a circular disk located 11” beneath the test section floor. Figure 20 is an AutoCAD drawing of the custom strut design used for the full scale wing. By using this new strut, we could mount the full wing in the tunnel. By allowing more than 12” of clearance we were able to reduce the presence of wall effects.

Figure 19. Image of Virginia Tech wind tunnel test section. The cross-sectional dimensions are 6’ x 6’.

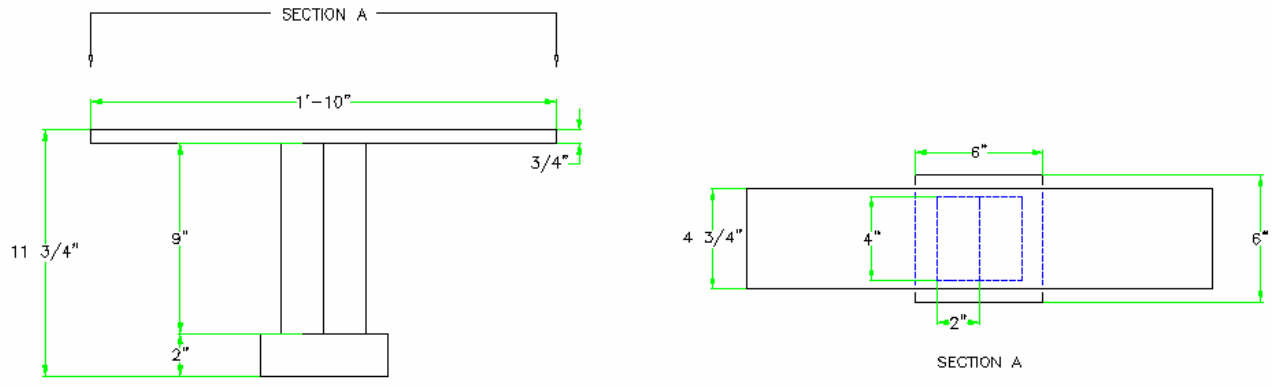

Figure 20. AutoCAD drawing of wind tunnel strut design. This strut was required because the wind tunnel cross-section was too small to use the existing strut.

To test the full scale wing the team needed to design a mock fuselage to store the actuation. We decided that a 16” wide fuselage, 8” per wing, would be adequate to store all the actuation and flight control components. Figure 21 is an AutoCAD drawing showing the approximate dimensions and shape for the mock fuselage. Since this fuselage was for wind tunnel testing only, weight was not a concern.

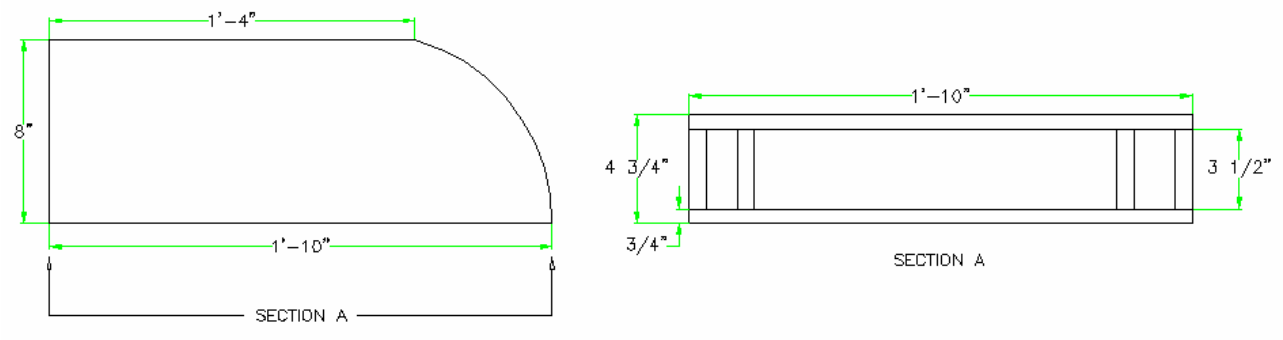

Figure 21. AutoCAD drawing of mock fuselage. The team allotted 8” of fuselage space for each wing.

3.5 Wing Sizing

It was desired that the wings undergo substantial changes in the chord, span, and sweep. It was required that the aircraft require reasonable take-off speeds. It was from these requirements that the wing was sized.

Span The built model would be tested in the Stability Wind Tunnel. The tunnel has a 6’x6’ test section, but a 1 foot clearance was required to avoid wall effects. This placed a restriction on the maximum half span of the plane of 5 feet. The amount that the span could increase was limited to a 14-inch extension due to the mechanisms. Four inches of the extension where then required to remain within the wing for structural reasons, producing a span increase of 10 inches. Due to the 5-foot total restriction, the minimum half-span length was determined to be 4 feet 2 inches.

Chord It was desired that the plane have a take-off speed between 20 and 30 miles per hour. The span being fixed by the tunnel and mechanical restrictions, the maximum required chord was calculated using the take-off velocity from Equation 1.

$$V_{LO} = 1.2V_{stall} = 1.2\frac{2W}{\rho_\infty S C_{L,\max}} \qquad (1)$$

A max Cl value was determined to be 1.0. This value was derived from experimental data of a Clark Y airfoil, shown in Figure 22. The Clark Y was used as a base airfoil because it has been proven to work with model airfoils, having high lift and low drag characteristics.

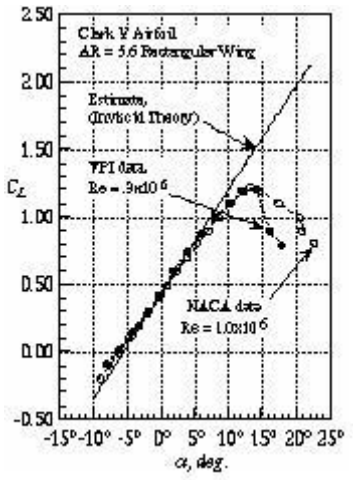

Figure 22. Lift coefficient versus angle of attack for the Clark Y airfoil [Mason, 2004].

The Clark-Y showed a max Cl value around 1.2. The max Cl value of 1.0 was then chosen as a somewhat conservative estimate. Using this value of Clmax and solving for the take-off velocity to be less than 30 miles per hour provided a max chord of 17 inches and a take-off velocity of 27 miles per hour. The mechanism for chord extension, however, was only able to accommodate a max chord length of 16 inches.

The minimum chord length was determined from cruise characteristics. It was desired that the aircraft cruise at Cl/Cd max and at a velocity between 30-35 miles per hour. This occurs at angles of attack between 2 and 5 degrees, but for these calculations, an angle of attack of 1 was used as a factor of safety. The Clark-Y has a Cl value of 0.5 at an angle of attack of 1 degree. These values were used with the velocity equation and generated a min-desired chord of 12 inches and a chord extension of 4 inches.

3.6 Airfoil Profile Design

It was required that the airfoil used would have a max Cl of at least 1.0. It was desired that the airfoil would have a late and controlled stall as well as low drag characteristics. In order to determine the airfoil to be used, three profiles were selected to be tested: Clark Y, Selig 8036, and Eppler 168.

Clark Y The Clark Y was selected as it is commonly used with model aircraft. It has shown that it has high lift and low drag characteristics. Using the Javafoil software to acquire performance estimates, the Clark-Y with chord retracted, shown in figure 23, generated a maximum Cl of 1.47 at 11 degrees angle of attack. The Javafoil software was used only for estimates and it is known to have an error up to plus or minus 10%.

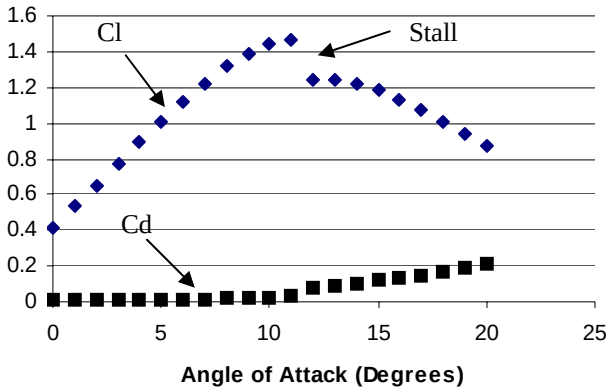

Figure 23. Plot of Cl and Cds for the chord retracted Clark Y

The Clark Y with extended chord, shown in Figure 24 below, showed reduced performance in that the maximum Cl was reduced to 1.16 and stalled at an angle of attack of 10 degrees. The reduction in Cl was to be expected as the thickness to chord ratio decreased, however, the overall lift of the wing increased due to the increase in chord.

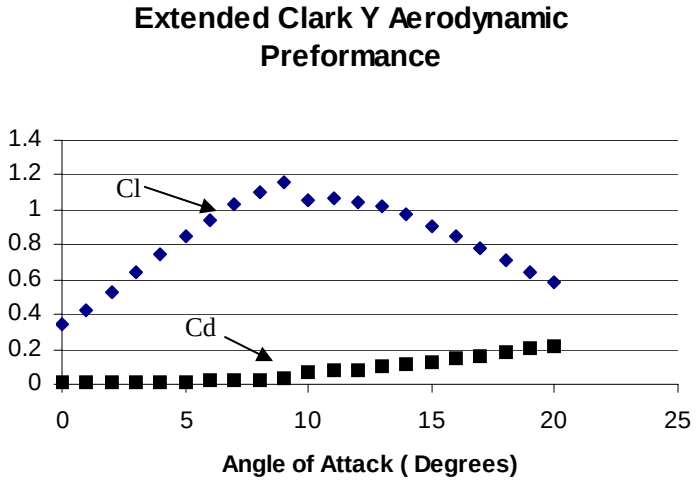

Figure 24. Plot of the Aerodynamic estimates of the extended Clark Y.

Selig 8036 One limiting factor on the choice of airfoil was that the airfoil had to be thick enough to fit the actuation systems inside. It was desired to test an aerofoil with a large maximum thickness in order to determine if the increase in thickness would substantially increase the drag on the airfoil. The Selig 8036 was chosen for this role as it showed impressive performance estimates as shown in Figure 25 below. The Selig 8036 estimates showed a maximum Cl value of 1.55 at an angle of attack of 15 degrees. The Selig 8036 showed a much smoother stall region occurring at higher angles attack than the Clark Y.

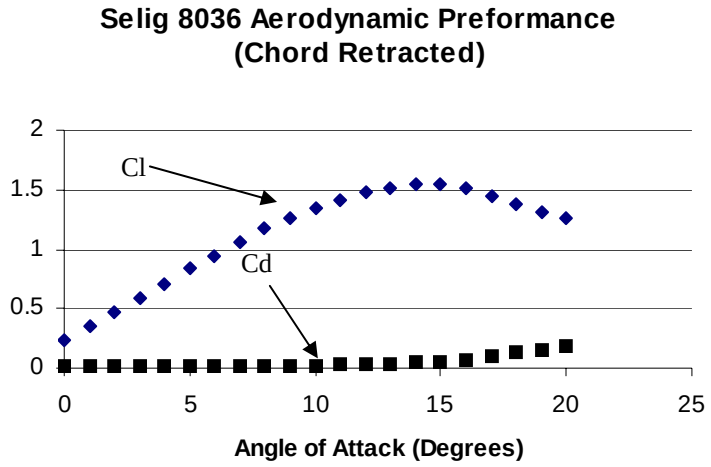

Figure 25. Selig 8036 Aerodynamic Estimates

The chord extended Selig 8036, shown in Figure 26, also showed excellent performance estimates. The extended Selig 8036 showed a maximum Cl of 1.25 at an angle of attack of 13 degrees. The stall characteristics of the extended version of the Selig were also smooth and controlled.

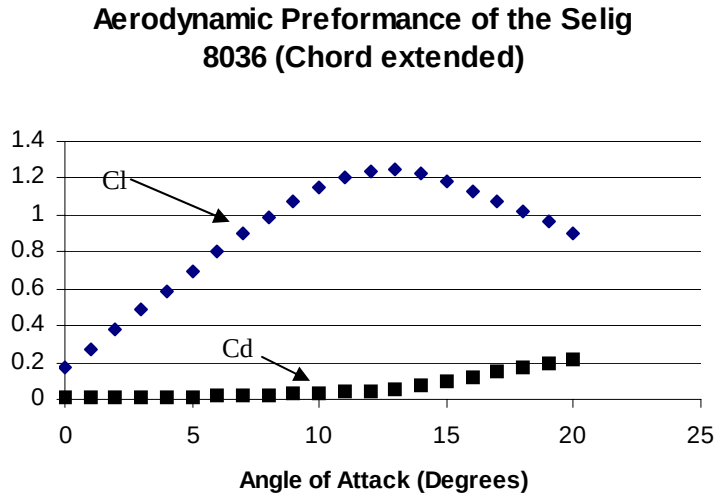

Figure 26. Extended Selig 8036 Aerodynamic Estimates

Eppler 168 The airfoil selected was also desired to have low drag. In order to test if sufficient lift could be generated from a low drag airfoil, the Eppler 168 was chosen. The Eppler 168, shown in Figure 27, showed an estimated maximum Cl of 1.01 at an angle of attack of 11 degrees. The Eppler 168 was estimated to have a smoother stall region than the Clark Y, but sharper than the Selig 8036.

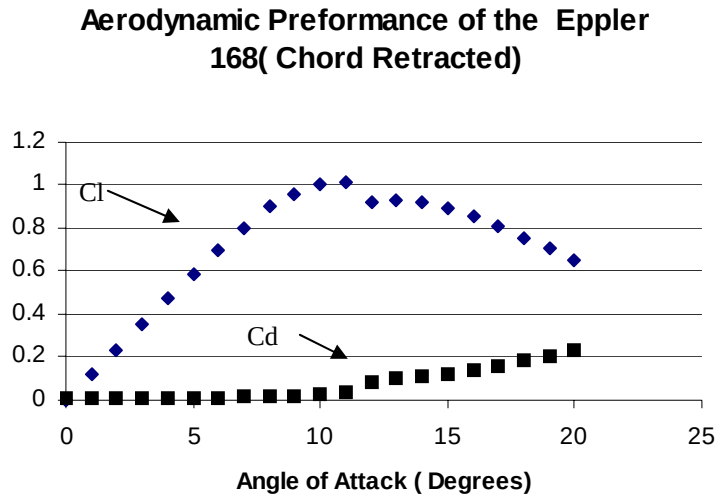

Figure 27. Eppler 168 Aerodynamic Estimates

The extended version of the Eppler 168 showed reduced performance with the maximum Cl reduced to 0.81 at an angle of attack of 9 degrees. The extended chord model also showed an increase in the drag coefficient as well a reduced stall angle of attack. Please refer to Figure 28 for the Eppler 168 aerodynamic estimates.

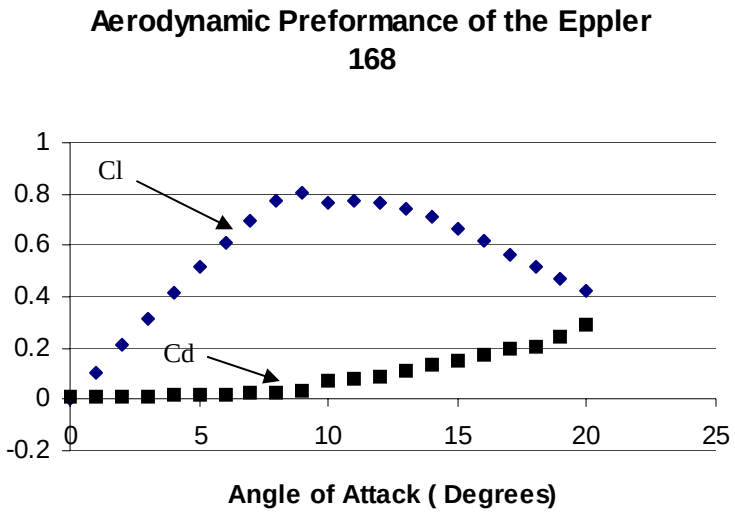

Figure 28. Extended Eppler 168 Aerodynamic Estimates

4.0 Model Construction

The following section describes the construction for the full sized wing wind tunnel model. The text details the physical construction of each component and shows images of each part taken during the construction phase of the project. The section starts with actuation and electrical systems and then proceeds to wind tunnel mounting equipment.

4.1 Actuation Construction

Sweep The first step in the sweep construction was to fabricate the sweep power screw block. The block itself was cut from a piece of dense plastic using a band saw. We then drilled out holes for the 1/4" power screw and the anodized metallic control horns. On each side of the power screw hole we mounted a single 1/4" nut with 30 minute epoxy. To reduce the friction on the power screw the nuts had to be perfectly aligned and properly greased. Figure 29 is an image of the sweep block upon its completion.

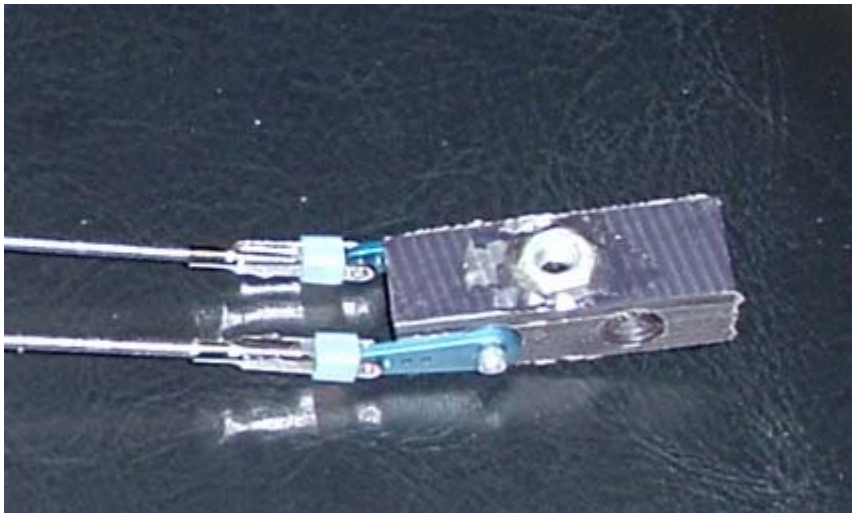

Figure 29. Image of sweep block. If the power screw nuts are not perfectly aligned with one another the threaded rod will not be able to rotate.

The next step in the actuation construction was to fabricate the mount for the servo/electrical system interface. The toggle switches used to control the sweep and chord motors are operated mechanically by two servos. To keep the servo arms at the right distance from the switches to activate them, we cut a mounting plate from a piece of plywood. We then cut holes to recess the two servos and the sweep and chord switches. To keep the control rods from slipping off of the switches we also used epoxy to mount a washer onto the top of each toggle switch. Figure 30 is an image of the plate with the servos and switches installed.

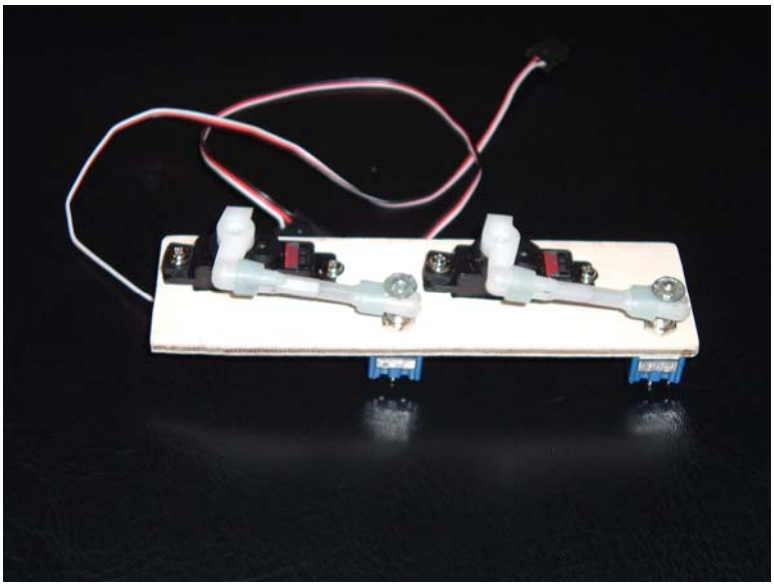

Figure 30. Image of servo/electrical interface. One servo/switch set operates the sweep morphing while the other operates the chord morphing.

To allow the entire wing to sweep back we needed to build a platform that could rotate on a pin. This turntable mechanism was constructed out of a piece of 1/4” plywood that we cut into a 16” semi-circle. We then trimmed the excess area to allow the plate to travel at larger angles. The sweep block was then connected to the turntable with a set of steel push rods and anodized control horns. Figure 31 is an image of the sweep mechanism within the mock fuselage.

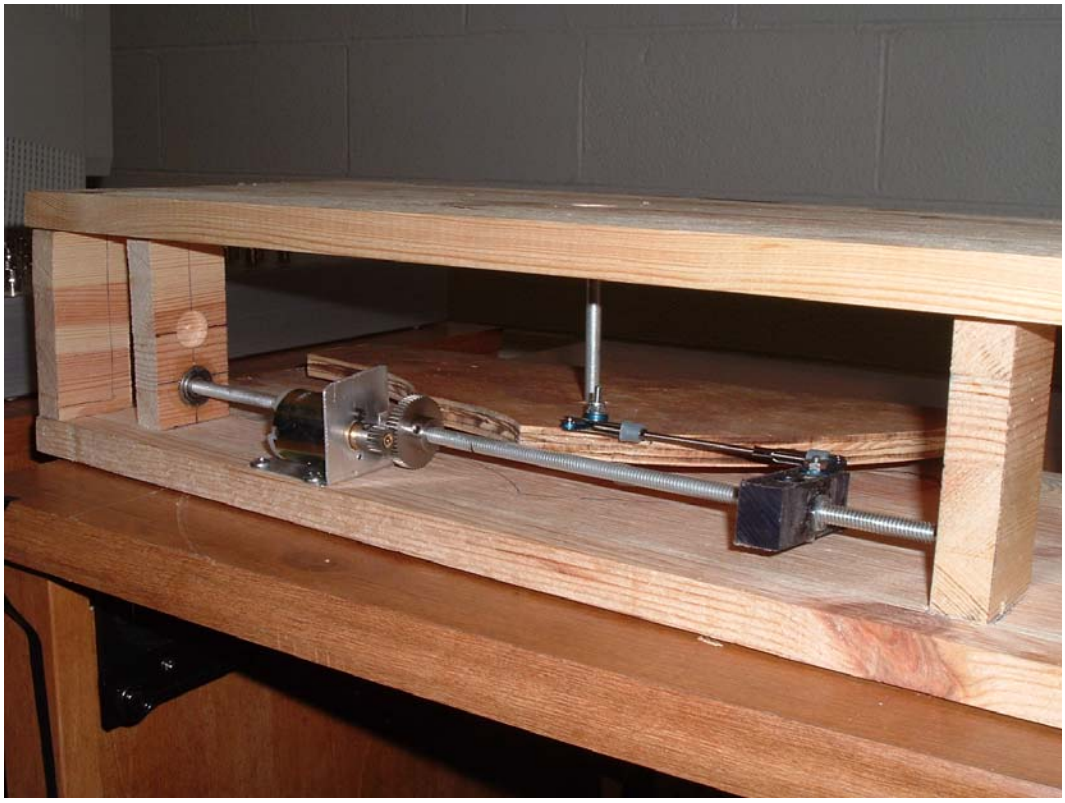

Figure 31. Image of sweep mechanism and mock fuselage. Details about the fuselage construction are discussed in more detail in later sections.

The majority of the chord mechanism was located within the wing. The chord mechanism construction began with the fabrication of three chord blocks. These blocks held the three individual power screws in place, allowing them to rotate but not translate. The blocks each have a 0.564” hole through them to allow the front spar to pass through. A second hole penetrates through the back side to allow a plastic bushing to be seated. A nut was then attached to the screw on each side of the bushing to hold it in place. These blocks were attached to the front spar using 30 minute epoxy. Again using epoxy we fastened a plastic 10 tooth sprocket to each screw right behind the chord block. Then we drilled a hole through the back spar and, like the sweep block, attached a nut

to each end of the hole. Figure 32 is an image of the Power screw and chord block before the read spar was attached.

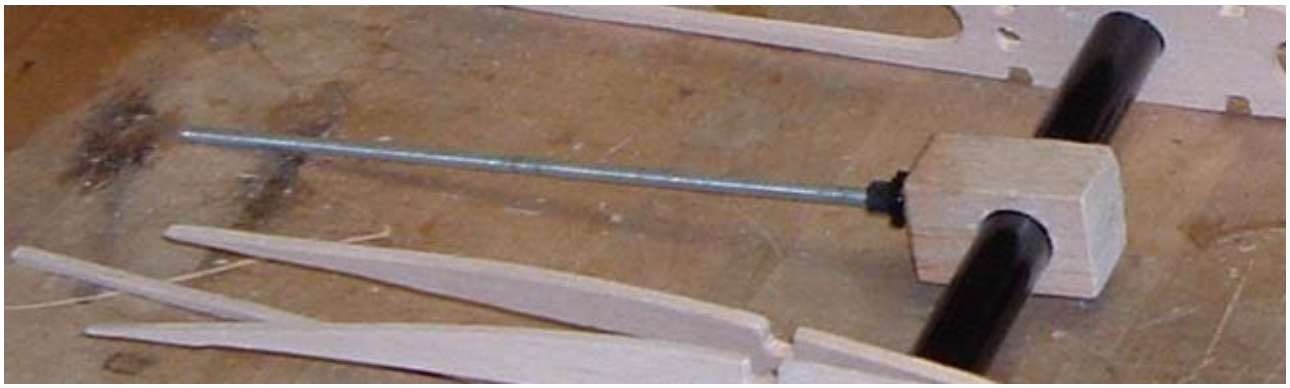

Figure 32. Image of chord block and power screw. This image was before the rear spar was installed.

On the turntable we needed to fabricate a seating for both of the main spars. The front spar was to remain stationary but the rear spar needed to translate a distance of 4” To hold the spars we cut a block and drilled a hole for the front spar. For the rear spar we attached an aluminum track that allowed a bolt head to slide through it. A bolt was then attached with epoxy to the rear spar so that the spar would remain perpendicular to the track at all times. Figure 33 is an image of the spar mount.

Figure 33. Image of spar mount. The aluminum track allows the rear spar to translate bud keeps the rod perpendicular to the surface at all times.

The span extension is much like an individual wing. The spar used for the extension was of the same high quality graphite as the others but was a slender 1/4” rod instead of a hollow tube. This gave the extension spar strength similar to that of the other spars but with a smaller cross-section. To allow the rod to move smoothly in and out of the front spar, two 1/4” linear bearings, like the one shown in Figure 34, where used.

Figure 34. Image of linear ball bearing. These bearings are fluent up to a deflection angle of 5 degrees.

To use the winch servo we drilled two holes through the extension spar, one through the middle and one near the base, for 50 lb test fishing line to pass through. To allow the servo to pull the extension out of the wing we ran the wire up through the wing using plastic cylinders as shown in Figure 35. By cutting a small hole through the front spar the servo was able to pull the extension from the center hole out of the wing. The lines were wrapped around the servo drum so that when the drum rotated the extension would extend and retract. Figure 36 is an image with the chord in and Figure 37 is an image with the chord out.

Figure 35. Image of span extension routing. To operate the span change 50 lb test fishing line was used.

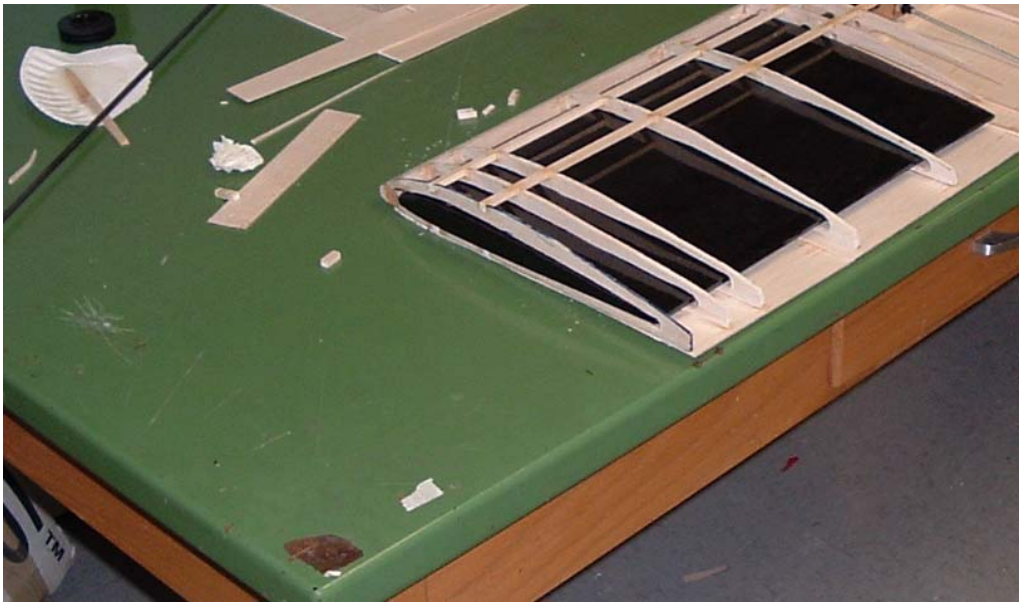

Figure 36. Image of wing with span extension in. There is no chord change where the span comes into the wing,

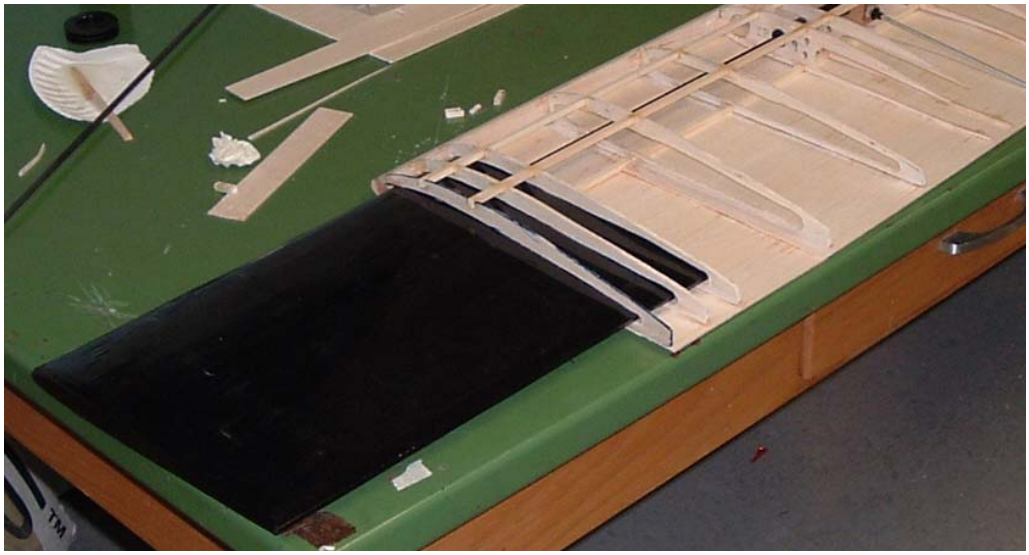

Figure 37. Image of wing with span extension out. Even at full span 4” of the extension remains inside of the wing.

To fasten the motors for the sweep and span change to the wing we cut and shaped a thin sheet of aluminum into a motor mount. The same type of motor and motor mount was used for both the sweep and chord actuation. Figure 38 is an image of the sweep motor mount with one of the electric motors installed.

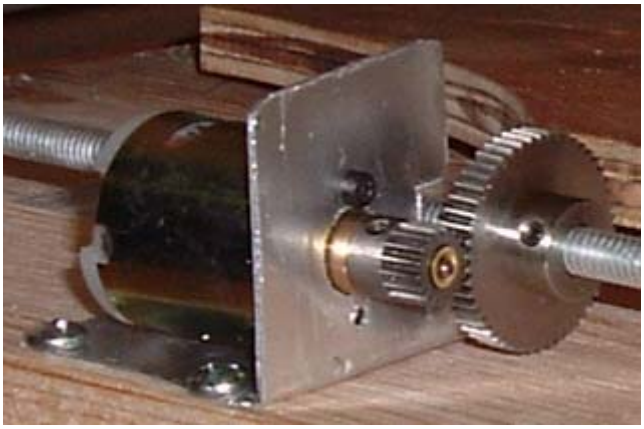

Figure 38. Image of sweep motor mount. Both the sweep and chord actuation use the same type of motor and motor mount.

4.2 Electrical Construction

Once the circuit diagrams were made in the design stage of the project, the construction of it was pretty straight forward. The compression switches were first attached to positions inside the mock fuselage as to where the actuation of the system would hit the switch, turning the circuit either on or off. For the chord change the two switches were placed on either side of the back spar where it anchored to the turntable. Since the back spar is the one that travels back and forth, the switches will be compressed at either side of its movement. See Figure 39 for a picture of the chord switch placement.

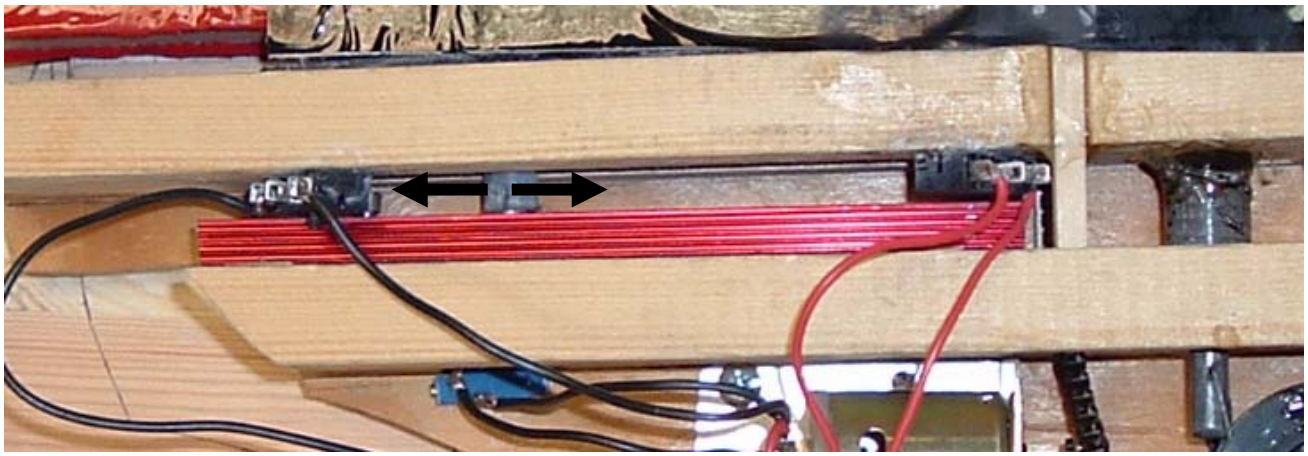

Figure 39. Chord switch placement. The spar triggers the switches as it slides up and down the aluminum track.

The switches for the sweep change were placed on either side of the threaded block that traveled up and down the sweep power screw. The wing was moved to its extremes at 0 or 30 degrees, and the switches were attached to the fuselage. Figure 40 is an image of the sweep switch placement.

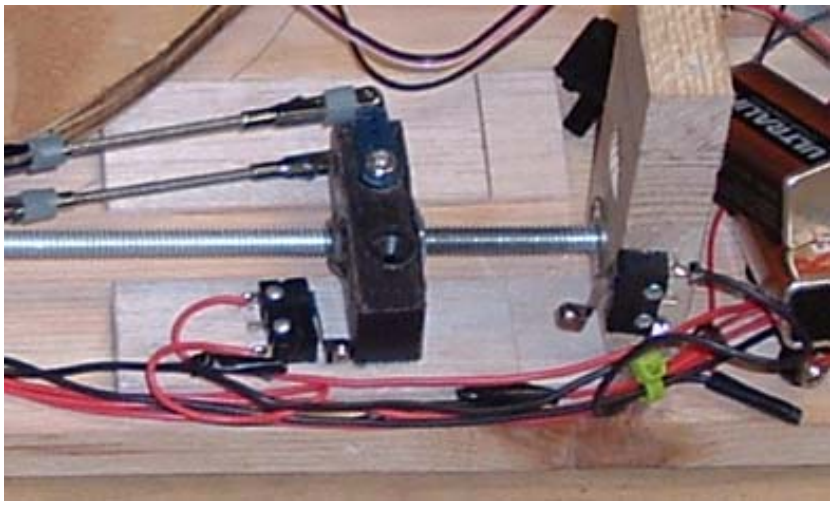

Figure 40. Image of sweep switch placement. As the sweep block shown moves to the right the wings sweep back.

Once these switches were in place and the position of the servo activated switches were secured, the wires for the circuit were laid out and cut to size. The wires were cut long enough so that they could be routed around any moving parts to prevent tangling. The wires were then soldered together and to the switches according to the circuit diagrams. The batteries used for the sweep and the chord change were two 9 volt batteries for each morph change. This is different than the battery used for the span change. Since the span change is actuated by a winch servo, a 7.2volt 1500mAmp 6 cell NiCad battery had to be used. The downside to this battery is it is very heavy for a battery pack, but the characteristics of it allow the servo to be used at its max torque.

4.3 Wind Tunnel Equipment Construction

In order to test our morphing wing design to see characteristics of it such as stall angle, it needed to be tested in the wind tunnel here at Virginia Tech. But because of the dimensions of our wing it would not fit into the stability wind tunnel using the strut provided. This required us to design and build our own strut that would attach to the angle of attack turntable.

As stated in the design section we were going to be building a block that bolts to the turntable which would attach to a strut which would extend up into the wind tunnel. The block that was bolted to the turntable was constructed out of a 6”x6” piece of pressure treated pine. This length and width of the block came from the position of the bolt holes on the turntable.

Each corner of the block had ½ inch holes drilled in them for the bolts. Each hole was ¾ of an inch from each corner. Since the bolts used for attachment were not long enough to bolt the block to the turntable, the bolt holes had to be recessed. The recessed holes aloud the bolts to sink down into the block leaving enough length of bolt to attach to the turntable

Since the turntable that the block was secured to is lower than the wind tunnel test section, a strut was needed to extend up into the chamber. The bottom of the test section is exactly 11 inches above the top of the turntable. Since we have a big wing that is going to be sitting on the bottom of the wind tunnel pointing up, we want to use all the space available. The block that is going to be attached to the turntable is 1.5 inches thick, so our team required a strut that was 9.5 inches in length to give us the height needed. The strut was constructed of two pieces of pressure treated pine 2x4s, cut at a length of 9.5 inches and then screwed together using four 3 inch drywall screws. The two pieces were oriented in a way that their 4 inch sides were butted up against each other. Please see Figure 41 for an illustration of the strut constructed and used. The block and the strut were then attached to one another using four 3 inch drywall screws.

Figure 41. Image of wind tunnel test strut. Wing must be mounted to the upper surface before the base can be attached.

4.4 Mock Fuselage Construction

Our morphing wing has a lot of actuation components with it that needed to be housed somewhere. Since this semester our team was building only one wing, a mock fuselage was needed to house the components that would fit inside the real fuselage. To simulate this fuselage a rectangular box was constructed with the wind-ward side having a curved front. The two sides of the mock fuselage were cut out of a ½ inch thick piece of pressure treated wood. First a rectangle with the dimensions of 22 inches by 6 inches was cut out of the wood. Then an arc with a 12 inch radius was cut out of the front so the fuselage was more aerodynamic.

Once the sides were cut out, the center was found where the swiveling turntable will attach. The turntable will attach using a ¼ inch diameter aluminum rod. In order to cut down the amount of friction when rotating, bearings were installed in each side of the box. Using a drill bit the same size as the outer diameter of the bearings, holes were drilled in the sides of the box to recess the bearings. In order to correctly space the two halves and connect them to each other, six 3 ½ inch blocks of work were cut out of a sheet of ½ inch thick pressure treated pine. The six of these blocks were placed throughout the two halves around the actuation. Two of the blocks were used to house the power screw used to actuate the sweep.

The bottom and the back side of the box were cut out of ½ inch plywood. Once the correct size dimensions were cut out to match the box, they were attached using 1 inch drywall screws. The bottom of the box was then screwed to the strut constructed using 3 inch drywall screws. When the time came to test the wing in the wind tunnel a $1/8^{th}$ inch piece of balsa wood was glued to fit the contour shape of the front arc. This was to create a more aerodynamic front and to protect the actuation components. Please refer to figure 42 to see a picture of the completed strut and mock fuselage.

Figure 42. Image of mock fuselage attached to wind tunnel strut. Curved side of mock fuselage points into the wind.

4.5 Full-Scale Wing Construction

Airfoil Selection Since the primary goal for the initial design was to test the morphing wing mechanism and the overall concept, the criteria used to select the airfoil section were not based on the aerodynamic performance. Rather the two criteria used to select the airfoil shape were based on the thickness to chord ratio to allow enough room for the mechanisms and the difficulty level to construct the airfoil section manually. Using these two criteria, the airfoil section selected for the full scale wing was the Clark Y, as shown in Figure 43. However, since the wing extension had to fit inside the main wing structure, the airfoil used for this section of the wing was changed to a Clark Y. This was done because; the tolerances needed to fit a scaled down Clark Y into the main wing structure and this could not be achieved with manual construction.

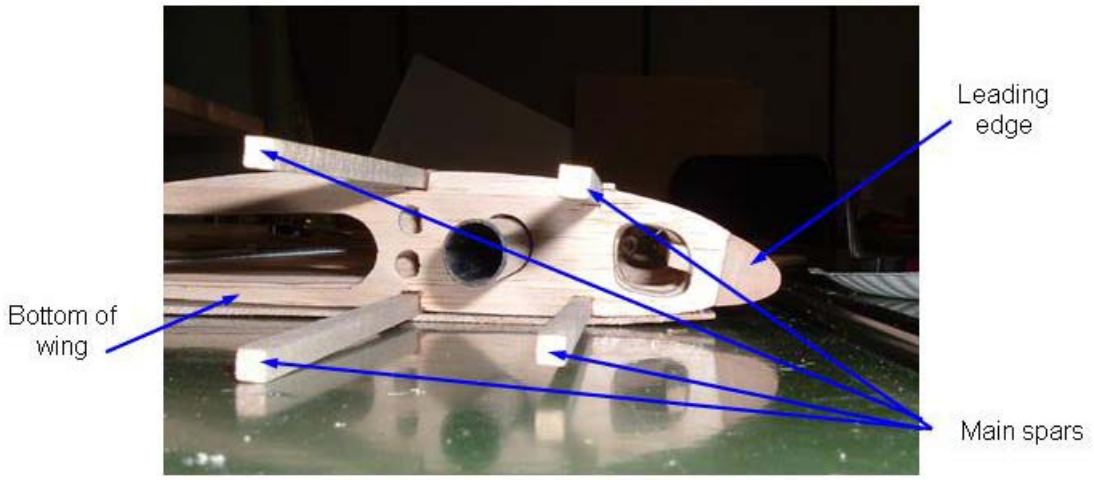

Figure 43: The cross-section of the full-scale wing showing Clark Y airfoil.

Construction To simplify the construction of the structure, the wing was built in three components. As shown in Figure 44, the three components were the main wing structure, the chord change structure and the span extension structure. The span extension was the first component that was built. The airfoil sections were made from 1/8” thick balsa wood and the main spars were made from 3/16” by 3/16” hard wood. The entire structure was then covered with 1/32” balsa sheets and then monokoted. After the span extension was built and covered, a template of the cross section was made. The template was then used to cut the housing for the wing extension located in the out board section of the main wing.

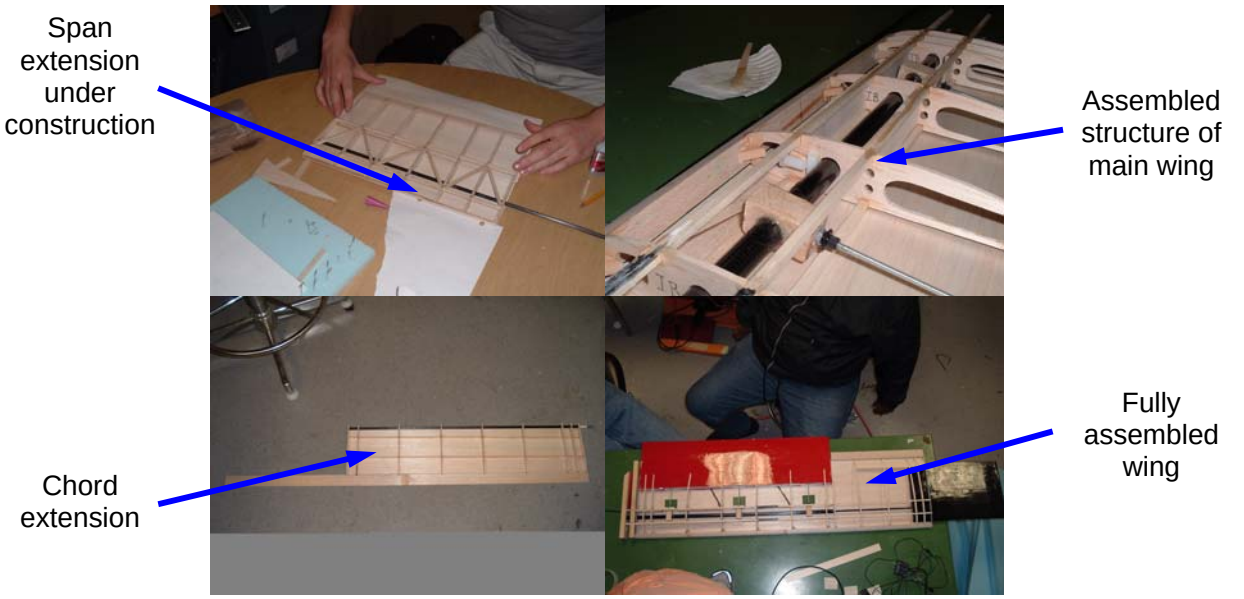

Figure 44. Four images of full wing construction.

4.6 Foam Airfoil Model Construction

The airfoil models were constructed from spider foam core models cut by flyingfoam.com. The foam core models were then covered with bi-directional carbon fiber sheets for stiffness. The carbon fiber was applied to the models with aerospace epoxy. Once the epoxy had dried, the fiber was cut flush to the models using the table jigsaw. The models were then finally sanded using a rotary sander and finished by hand for smoothness.

The quality of each model was not uniform. Several models needed epoxy repairs for locations where the carbon fiber had been worn through from over sanding. The smoothness of all the models also was unequal and the quality of the smoothness across the same airfoil was not uniform. The trailing edges of each airfoil were by far the roughest section as the majority of time was spent insuring the smoothness of the leading edge.

5.0 Wind Tunnel Testing of Foam Models

This section describes an experimental study of the longitudinal aerodynamic characteristics of the six models constructed. The main objective driving this test was to examine the separation

pattern over the wing in its extended-chord configuration. Runs of the applet JavaFoil for the extended airfoil geometry predicted separation at the location of transition between the front part of the wing and the extension, even for very low angles of attack. However, the results obtained were considered to be highly questionable since such computer codes are not suited to handle sharp angles as the one presented by our design. Therefore, it was decided to test the airfoil geometry in the wind tunnel to determine if separation actually occurs. It was also decided to test the standard (retracted) configuration of each airfoil to obtain our own data corresponding to flow conditions and wing geometry of the morphing airplane in loiter configuration. Ultimately, a comparison between data obtained for extended and retracted versions of a same profile served to determine the worthiness of the morphing chord-extension concept.

A total of six unswept, untapered wing planforms with a 4 foot span and a 0.64 foot chord were thus subjected to experimental study in wind tunnel. The experiment was conducted in the Virginia Tech Stability Wind Tunnel.

5.1 Experimental Goals

The goals of this study were:

1. To examine the performance and flying characteristics of the models.
2. To examine the separation pattern on the extended-chord airfoil models.
3. To compare the aerodynamic characteristics and stall behavior of the three extended-chord models.
4. To compare the aerodynamic characteristics of original and modified version of each airfoil.

5.2 Foam Model Test Procedure

To attain these goals, a sequence of 25 runs has been conducted with the models placed in the closed test section of the wind tunnel. For each model longitudinal tests with angle of attack sweep from approximately -6 to 22 degrees by steps of 2 degree increments, were performed for several tunnel speeds and the objective was to determine:

- lift curve slope
- angle of attack at zero lift

- maximum lift coefficient
- maximum usable lift
- aerodynamic center
- nature of the pitching moment curve “break” near stall
- zero lift drag
- drag due to lift performance relative to the 0% and 100% polars

In this test campaign, six models had to be tested. Since the wind tunnel time available for this campaign was limited to approximately 10 hours, the procedure was a critical aspect for the testing organization.

In order to reproduce the flow condition at various flight stages, the tests were done at three different Reynolds numbers. The lowest corresponds to the full scale aircraft take off flow conditions, the middle to a low cruise speed, and the highest to a faster cruise condition. The tests corresponding to these Reynolds number were referred respectively as Low Speed (LS), Middle Speed (MS), and High Speed (HS). These different Reynolds number were chosen to investigate a broad range of Reynolds number values and to see its effect on the aerodynamic performances.

The tests were done one profile shape after the other. For each profile, the retracted version was tested before the extended. This procedure allowed analyzing the extended version based on the performance of the retracted version. To have a better understanding of how the tests were organized, the flowing flowcharts in Figure 45 have been designed. They represent the logical decisions that had to be applied in order to fulfill the goals stated earlier.

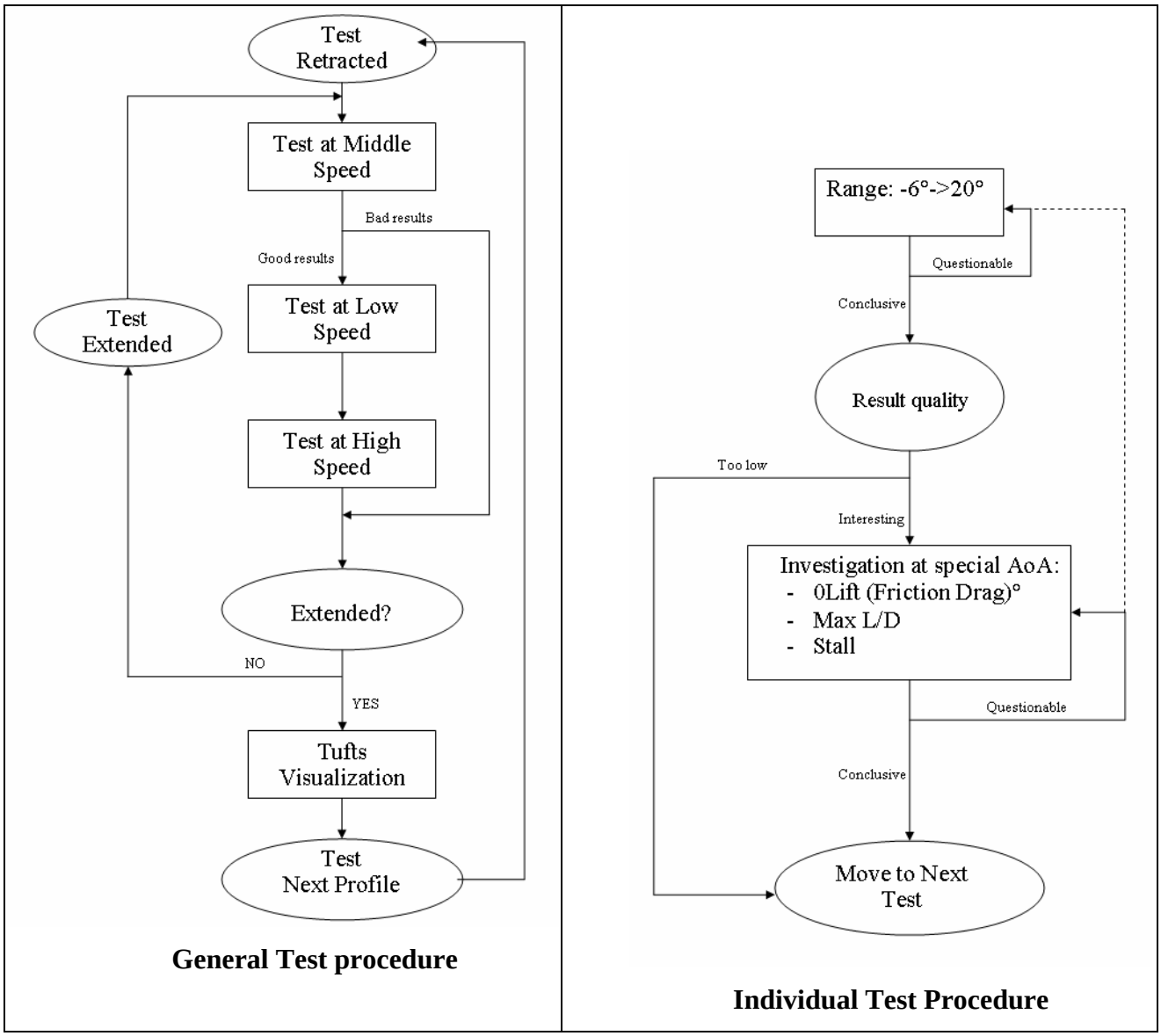

Figure 45. Flowcharts of test procedures for foam wind tunnel models

Concerning the individual test procedure, the general approach was first to make a run covering angle of attack between -6° to 20° with 2° increments. After this run, a quick analysis of the results was done to locate the zero lift angle of attack, the max L/D angle of attack, and the stall angle of attack. Investigation at zero lift was to measure the friction drag and the measurements at the other angle were done to explore the performance of the model. On the flowchart, the conclusions "conclusive" and "questionable" relates to instrumentation mishaps or grossly unrepeatable results. After the general tests, in order to avoid spending more wind tunnel time on unnecessary tests, the general measurements were analyzed and benchmarked to see if the model's performance was worth to be investigated.

The theoretical aerodynamic and technical characteristics of the CLARK Y have shown that it was the best candidate for the wing; therefore, priority was given to the tests of the CLARK Y models. Also, to produce a reference that would validate both the wind tunnel instrumentation and the carbon fiber model, the first model tested was the traditional retracted CLARK Y wing. Having tested a modified CLARK Y in previous experiments, data was available to compare and evaluate the resulting aerodynamic characteristics.

Therefore, the tests on the traditional CLARK Y model were not only dedicated to determine the aerodynamic performance of the model but also:

- To validate the readings of the wind tunnel strut by comparing the reading to previous tests and validating them by recognizing similar patterns in the amplitude of the resulting forces, their evolution and their repeatability.
- To show that the models had aerodynamic characteristics similar to previously tested model. Since the coating of the models were not perfectly smooth, it was important for the test to recognize its effect on the aerodynamic performance.
- To analyze in an organized and detailed manner all the results that could be gathered during the experiment, this part of the report will be organized in three parts:
- Lift Coefficient analysis
- Tufts visualization and analysis of separation
- Aerodynamic performance for flight of the models

During the 23 wind tunnel runs that had been operated during this experiment, voluminous amounts of data were accumulated. Due to defective equipment, some runs did not produce realistic or repeatable measurements. Before presenting the results it is important to note that the data could not always be processed directly from the measurements. Therefore, the major impact of this equipment limitation was the loss in accuracy of the measurement. In order to restore the precision to an acceptable level, the data was averaged for repeated runs. The impact of that technique was that the investigation about speed effects on the aerodynamic performance was lost in order to increase the number of trials needed to make a statistical improvement of the accuracy. But this decision was inevitable because the speed or Reynolds number’s effect on the performance fell deeply under the level of repeatability. Therefore, it was impossible to quantify the effect of the Reynolds number from the original measurement.

5.3 Foam Model Test Results

The results that are going to be presented and analyzed in this report are representing the average (unless specified) of the models characteristics over the speed at which the aircraft is going to be operated.

First the lift coefficient that could be obtained from the models will be analyzed. Since the goal of this experiment was both to explore the aerodynamic performance of the models and to compare the extended model to the retracted, two different lift coefficients are going to be defined.

To analyze the characteristics of a model independently, *CL* is going to be used. This *CL* is the non-dimentionalized lifting force defined by equation 3. The chord that is used in this equation is the actual chord of the model. Since all of the models have the same dimensions, the chord length used is 7.68".

$$CL = \frac{L}{q \times b \times \bar{c}} \qquad (3)$$

In order to have lift coefficients in the same scale for both the retracted and extended models, the lifting forces were also non-dimensionalized in a different manner. For the extended version, the reference chord did not correspond to the actual physical chord of the model. For the aircraft, the reference chord is the retracted chord. Therefore the reference chord of the extended model was ¾ of its physical chord. The lift coefficient *CL** was then defined by:

$$CL^* = \frac{L}{q \times b \times \bar{c}_{\min}} \qquad (4)$$

Note: For the models representing the wing chord retracted, *CL*=CL* and for the extended chord models, *CL*=4/3 CL*.

The lifting characteristics of the model are presented on Tables A1, A2 and A3. In these tables *CL* and *CL** are associated to their corresponding angle of attack α, and their angle from the zero lift angle of attack, α^* ($\alpha^* = \alpha - \alpha_{0L}$). The symbol α^* is used is because it shows the angle of attack in a tangible reference frame. The angle of attack α, can not be defined with certainty because α=0° could not be measured accurately during the tests. Also plotting the lift coefficient with respect to α^* allows better comparisons between the curves therefore improving the clarity of the figure for analysis. The data listed in Tables A1, A2 and A3 are respectively plotted in Figures A1, A2 and A3 as *CL** versus α^*.

5.4 Effect of Chord Extension on Aerodynamic Performance

Plotting *CL* (not *CL**) versus α^* for the modified profile (see figure A7) and comparing it to the equivalent plot using the unmodified profile *CL*'s (see figure A8), we can see that the lift amplitude and characteristics of each profile are similarly damped.

On figure A8, one can recognize the geometrical characteristics of each profile from their impact on performance. The slope of the lift curve is strongly proportional to the thickness to chord ratio. In this figure we can see that the Eppler slope is the highest, followed by the slope of the Clark Y and that the Selig has the lowest slope. Geometrically, this order coincides with the thickness to chord ratio of these profiles. On figure A7, we can see that the slope effect is strongly decreased for the extended chord curves. All three models have slopes that are close to each other. This could be explained by the fact that the thickness to chord ratio difference between the modified models decreased, since the thickness of the models remained the same while the chord dimensions increased.

The modification done on the profile for the chord extension had a similar effect on the stall point. The unmodified model had a very different stall pattern. The Eppler had a short transition before stall, and the Clark Y and the Selig had a sharper stall. These patterns were also predictable from the geometric characteristics of these profiles. The Eppler had a thick and round leading edge that is known to allow smoother stall characteristics. The angle at which the retracted models start to stall is also different for each profile. The Eppler starts stalling at α^* values of 6° while the other two profiles keep their lifting performance up to values around 13°. The stall pattern of the modified profile agrees with the original stall pattern because the extended Eppler also stalled earlier than the other two, but once again the difference is less sensible. On the other hand, the stall pattern of these modified versions differed on an important aspect of the stall. It is recognizable that all three models have a transition range on the angle of attack. Over this range the lift stays constant with the increasing angle of attack. This stall characteristic was not expected and adds value to the design of the chord extension.

5.5 Lifting Performance of the Modified Profile

This procedure for chord extension was designed to generate high lift that would allow take off with a smaller wing dimension. Therefore, it is desired to know whether this procedure

produces more lift than the original profile. To be able to compare the different characteristics of the lift curves, figure A5 shows a plot of CL* versus α and figure A6 shows CL* versus α*. It is noticeable that the chord is producing significant improvement in lift. Analyzing the data defining these curves, the histograms in Figures A9, A10 and A11 could be constructed. These important values are also listed in Table A5.

As stated earlier, the chord extended wing should be a configuration specifically aimed at take off and landing. For these flight conditions, the wing should generate the largest *CL** possible in order to take off (or land) at the lowest speed possible. Therefore, the maximum lift available is a critical parameter of the wing because it is going to determine directly the take off and landing speed for the aircraft. Also for these maneuvers, the wing should be able to produce a different amplitude of lift for a small change in α. At take off, changes in α correspond to rotation or a pitching up of the aircraft nose. For a given wing bank on an aircraft, the rotation angle is inversely proportional to the CL^*_α. Therefore, a large CL^*_α is beneficial for the take off performance. Figure A6 presents a measurement of the stall resistance of each model. The symbol $\Delta\alpha_{max}$ is defined by the difference between the α at which the lift is no longer varying linearly and the zero lift angle of attack (α_{0L}). This range allows evaluating the stall resistance of the wing. This stall resistance is a major characteristic of the performance of the wing because it provides maneuverability, and security against stall in high lift flight conditions. The ranking of the possible profiles based on the criteria listed above puts the Clark Y-e first before the Selig-e and the Eppler-e.

After preliminary analysis, using different flow simulation software, it was difficult to predict the behavior of the flow around an airfoil shape that is unique in its profile shape. The main concern about the aerodynamic characteristics of the modified profile was concerning flow separation around the physical transitions between the two bodies constituting the wing. These transitions induce “sharp” concave and convex corners which could have an effect on the flow that was difficult to predict. Preliminary analysis predicted a stagnation point in the concave corner that could initiate a separation bubble and a strong adverse pressure gradient on the convex corner that would separate the flow. Separation was a critical concern because it would eliminate all benefits from the chord extension. The flow visualization done using tufts cleared the design from these negative assumptions.

The separation pattern as seen on the tufts is described by figure A12. For small α*, the flow is completely attached. No special turbulent or stagnation point could be observed on any corners of the profile transition. The only turbulence to be seen at low α was induced by the screw

connecting the model to the test strut. For the α range on which the flow is varying linearly, separation develops slowly. The separation starts from midspan in the wake of the screws. This separation "pocket" progressively grew with α until the end of the linear region. This separation pocket is from the trailing edge to approximately half the chord of the model. As α increases, the pocket grows toward the wing tips on the sides. After the linear growth of the lift coefficient with respect to the angle of attack, the separation pocket stabilized. At this stage, the flow at the trailing edge is separated over almost half the span of the model. For an α range of 4 -5°, no change was seen on the tufts behavior. Therefore no change in flow separation occurred for this range of α. Over this range, the lift coefficient stayed constant. After this transition range, the flow separated violently on both tips of the model simultaneously. This separation clearly characterized the final stall of the profile. This final stall occurred at an angle that was equivalent to the stall angle of the retracted versions. The transition stage prior to stall was in a sense subtracted from the α-range of the original profile. This transition has both its advantages and drawbacks. It is beneficial in the sense that is can be a "pre-stall" signal to the pilot. If he increases the angle of attack of the aircraft and does not feel any benefit from it, it will be a warning against stall. But on the other hand, it is taking on the maximum lifting performance of the wing. As described earlier this transition occured at a range of α* over which the original profiles kept increasing their lift coefficient.

Pictures from a test done in April 2004, during flow visualization, showed the flow separation pattern on a modified Clark Y. These pictures are presented in Figure A13. It is illustrated in these pictures that the same separation pocket starts from the trailing edge mid-span, and then grows towards the tip of the model. A major difference is that the flow tends to separate more easily on the trailing edge, at the tip of the wing, more so than the extended model. For the extended versions, separation did not occur anywhere at the tips before final stall.

Due to instrumentation issues, the data available about the *CD* and *CM* are limited. The gage reading these parameters was either not configured properly or the gage itself was broken. Between different runs the variance was so large that it displayed two values for the same measurement and they would differ by up to a factor of two. Figures A14 and A15 show the *CD* and *CM* values for the retracted Clark Y as measured during two successive and identical runs (runs 3 and 4). As one can see the measurements are very different from each other. The only thing that can be analyzed from this data is the slope of the pitching coefficient. Assuming that the measurements are somewhat proportional to the actual value of the pitching moment, Figure A16 can be analyzed by looking at the general shape of the curves. On this figure the measurements for

the Clark-y and the Selig (extended and retracted) are represented. Since the measurements of the Eppler models seemed so erroneous, with variation of CM from -2 to +20, they are therefore not represented.

Figure A16 shows the pitching moment *CM** taken at the quarter chord of the models. This plot shows that the extension did not modify the pitching moment slope. The stability behavior is thus not drastically changed. Therefore, it should be expected that the extended models will have similar *CM**behavior to their retracted versions. Since the value and the slopes of the *CM** curves are meaningless due to the data acquisition system, it is difficult to make any reliable observation and analysis from this data.

6.0 Wind Tunnel Tests for Full Scale Wing

6.1 Experimental Setup

Due to the size of the full-scale wing, it was not possible to use the same experimental setup used to test the foam models in the stability tunnel. To mount the wing vertically in the tunnel it was necessary to remove the strut and devise a new mounting setup for the wing. The new mounting setup, which was custom made in the CIMSS lab, had four components as shown in Figure 46. The four components were the mounting plate, height adapter, cover plate and wing attachment plate. Various types of wood and three inch standard screws were the material used to build the mounting setup.

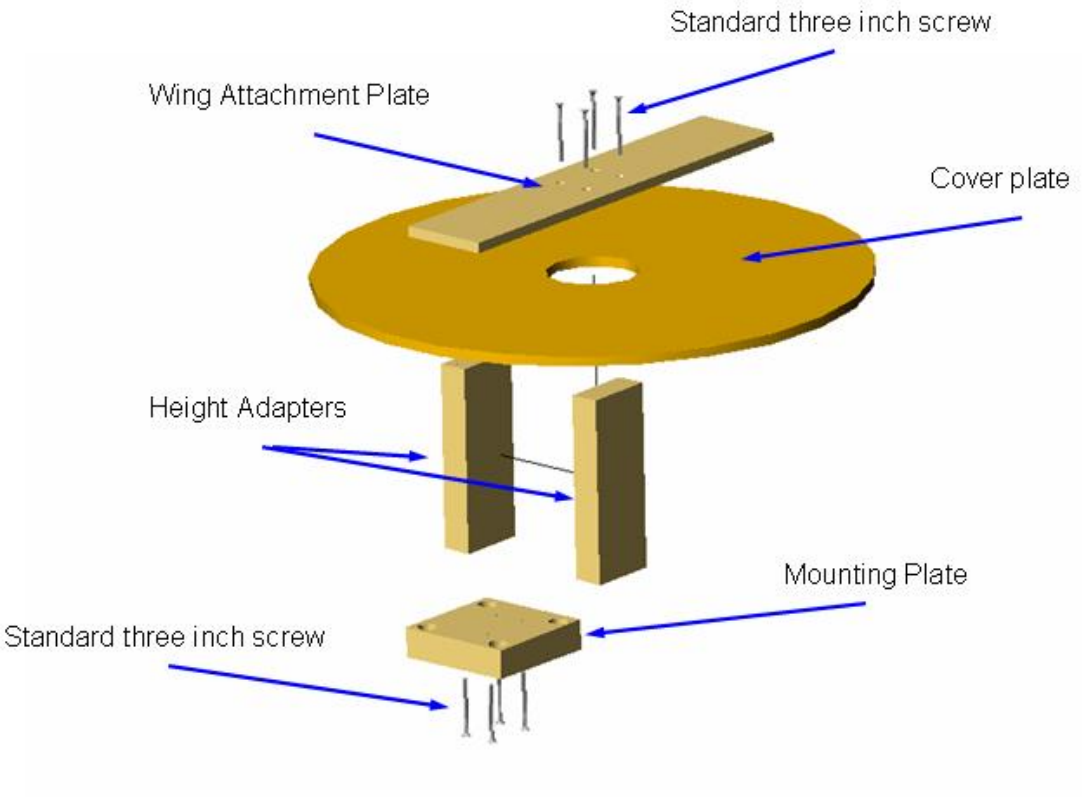

Figure 46: Schematic of new mounting setup

It is important to note that when the strut was removed, the data acquisition system and the automated system used to change angle of attack were also removed. An attempt to build a new data acquisition system for the new mounting system was not possible due to the complexity and time need to undertake such a task. However, the automated angle of attack system was replaced by using the wing tunnel's turn plate, which is normally used to change the sideslip angle, as a mechanism to change the angle of attack. For the experiment setup shown in Figure 47, the counter clockwise rotation of the turn plate corresponds to positive angle of attack and clockwise rotation corresponds to negative angle of attack. Figure 48 shows the turn plate and its mechanism.

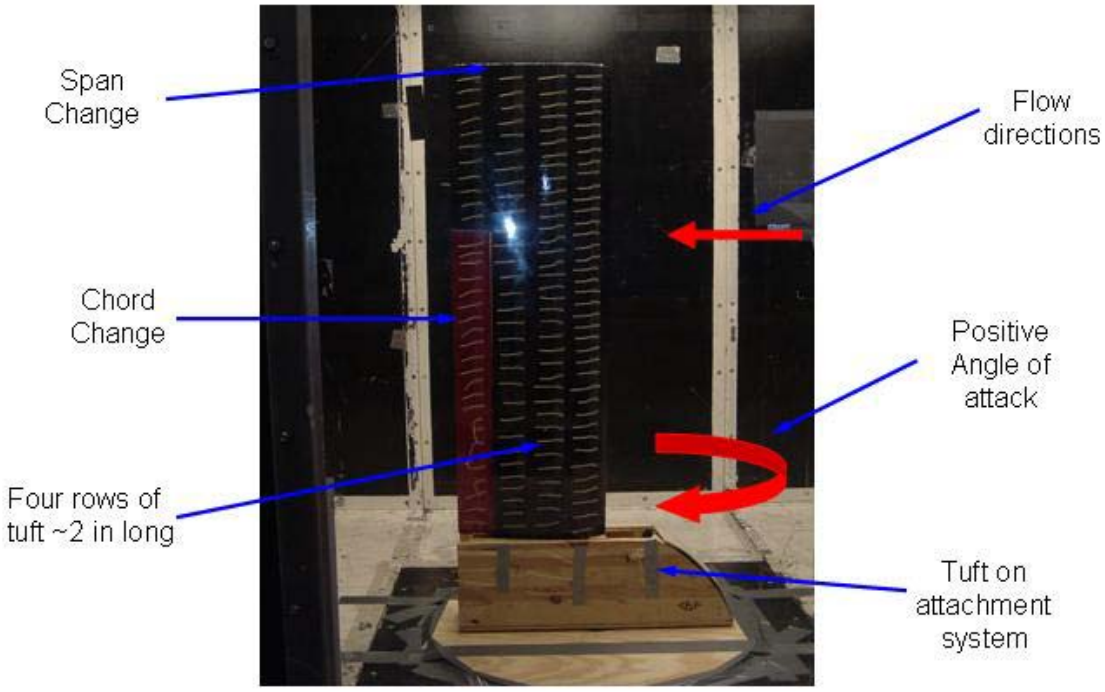

Figure 47: Experiment setup for full-scale wing tests.

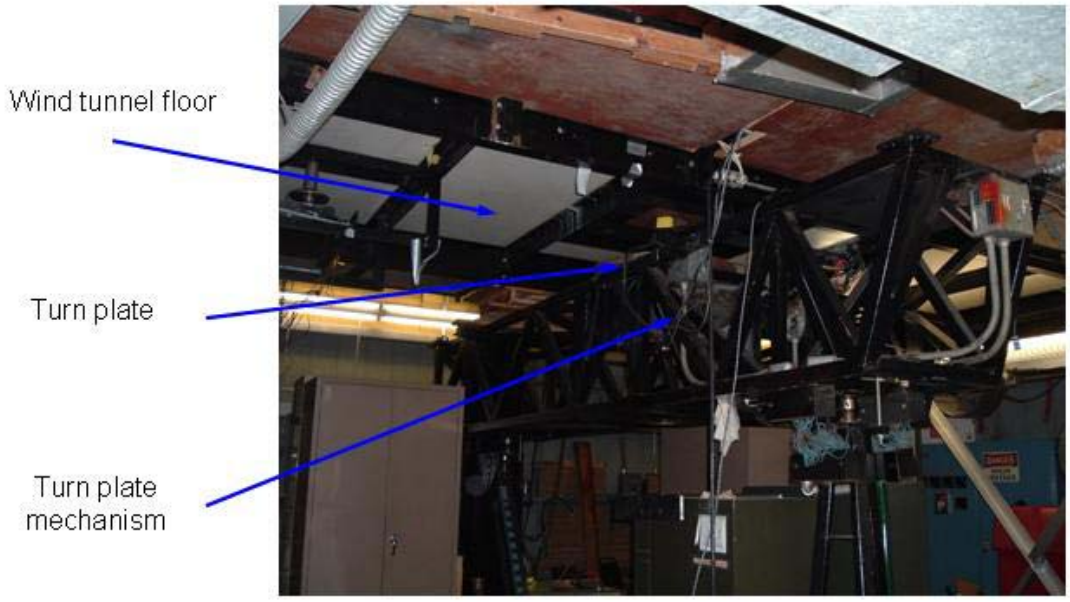

Figure 48: Wind tunnel sideslip turn plate and mechanism

In addition, since there is on data acquisition system a method for approximating the angle of attack for the wing was devised. This method involved marking straight lines at increments of 5 degrees on the cover plate and approximating the angel by observing down from the tunnel test-section roof.

6.2 Pre-Test Matrix of Goals

The primary goals of the tests were to prove that the wing can morph under aerodynamic loads and to conduct flow visualization for different configurations of the wing. The speeds of the tunnel were chosen based of the estimated take-off speeds for the morphing wing aircraft, which is scheduled to be built in spring 2005 semester. As shown in Table 1 there were five pre-test goals set for testing the full-scale wing. The first four tests were setup so that the flow visualization results for the full-scale wing and the foam models can be compared. The last test case was setup to determine weather the new mounting system affected the flow over the in board section of the wing.

Table 1: Pre-test matrix for full-scale wing.

SPEED AND ANGLE OF ATTACK

Test velocity = 30 -35 mph (Takeoff speeds)

Angle of attack range = 0 – 25 degrees

TEST CASE	TEST DESCRIPTION
1	Flow visualization for NO span and NO chord change, normal wing. Determine approximate stall angel of attack
2	Span change under aerodynamic loads and flow visualizations for span extended configuration. Determine approximate stall angle of attack
3	Flow visualization for chord change configuration. (Chord extended before starting test) Determine Approximate stall angle of attack
4	Flow visualization for span and chord change. (Chord extended before test and span extended during test.) Determine approximate stall angle of attack
Special case	Look at flow interaction between Mounting system and in board section of wing.

6.3 Problems during Wing Tunnel Tests

In attempting to conduct the tests, as stated in Table 1, a number of problems were discovered. The problem, which significantly affected the test, was the wings sweep mechanism. As the speed in the tunnel was increased and the aerodynamic loads started to take effect, the wing started to move about the sweep pivot point. This motion was not large enough to cause concern at first, however increasing the angle of attack to conduct flow visualization test increased the aerodynamic loads and the motion of the wing was magnified. For the safety of the model and the tunnel, it was necessary to abort the test after reaching a speed of 20 mph. An examination of the pin for the sweep pivot point and the sweep change mechanism reveled that the sweep change mechanism was the cause of the problem. Further, the repairs necessary to correct the problem

required removing the wing from the tunnel. This was because of the location of the sweep mechanism as shown in Figure 49.

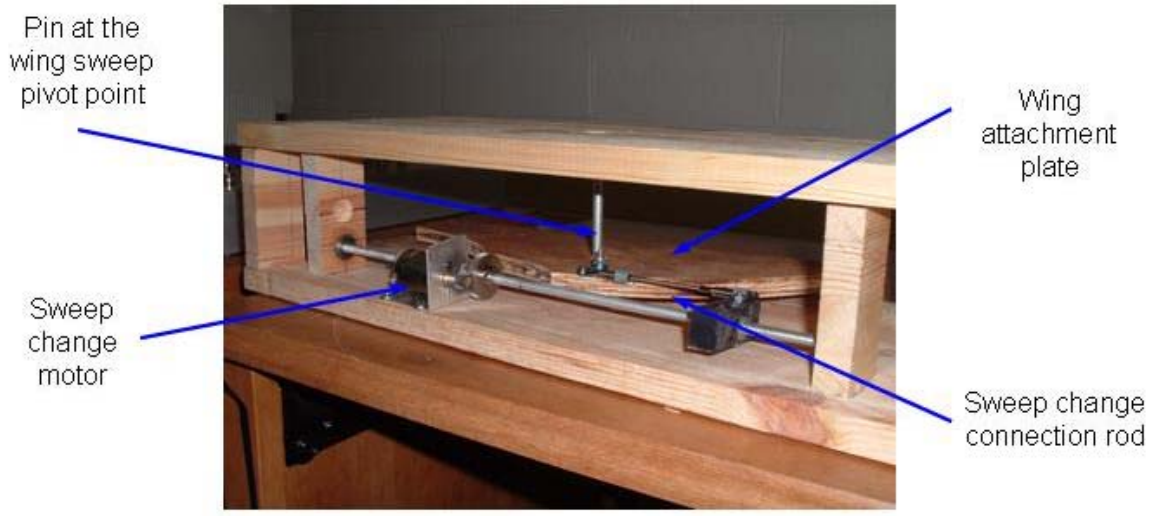

Figure 49: Sweep change mechanism for full-scale wing.

Since removing the wing from the tunnel for repairs would have wasted valuable time from the test, it was necessary to modify the method of testing. The first approach used was to change the angle of attack at low speeds and then increase the speed to the specifications of 30 to 35 mph. This approach did not work because the wing stated to move considerably at a speed of about 25 mph and it was necessary to stop the test.

The second approach used was to modify the pre-test matrix in order to accomplish some of the goals. From the initial set of tests, it was apparent that changing the angle of attack caused unacceptable amount of motion. This meant that for test cases one though four determining the approximate stall angle of attack was not possible. Taking this into account the modified test matrix shown in Table 2 was created.

Table 2: Modified test matrix for full scale wing.

SPEED AND ANGLE OF ATTACK

Test velocity = Variable

Angle of attack range = 0 degrees relative to flow

TEST CASE	DESCRIPTION
1	Determine the maximum speed for tests by increasing tunnel speed in small increments. NO span or chord change for this test.
2	Morph the wing under aerodynamic load using speed range from test case one with NO chord change.
3	Flow visualization for chord change with NO span extension .
Special case 1	Wing tip vortices for normal and span extended configurations.
Special case 2	Look at flow interaction between Mounting system and in board section of wing.

6.4 Full-Scale Wing Results

The modified goals stated in table 2 were successfully tested with no further problems. Table 3 shows a summery of the results. A summary of the test conditions acquired from the stability tunnels instrumentation is shown in Table 4.

Table 3: Summary of test results

TEST CASE	RESULTS
1	The maximum speed for the un-extended wing a zero angle of attack was around 36 mph.
2	Morphing tests on the wing were conducted by extending the span via a remote control at speed around 25 and 35 mph.
3	Flow visualization for chord change, tested around 35 mph showed no separation.
Special case 1	An interesting observation regarding wing tip vortices was made when the span was extension was fully deployed. The tuft on the wing extension showed that there was no wing tip vortex. However, the tuft attach to the un-extended wing tip showed that was a wing tip vortex
Special case 2	No significant effects were seen on the in board section of the wing due to the mounting system.

Table 4: Test conditions.

Date: Thursday 11/18/04 4:45 AM
Tunnel Temperature: 64.6 ^{o} F
Outside Temperature: 52 ^{o} F
Pressure: 28.01 ins of Hg

7.0 Conclusions

7.1 Actuation Conclusions

In conclusion, this project was an overall success. We may not have met all of the goals that we set at the beginning, but with failure comes the opportunity to see what will and will not work. The span change that was actuated by a winch servo performed perfectly. With the movement of the radio transmitter joystick the span would move out at a reasonable speed. It was also able to

contract to a compressed wing shape just as easily. Where our team ran into problems was with the chord and sweep change.

The chord change power screws in the wing were a little difficult to turn using the chain. This was due to using plastic bushings on the spar-screw connections and not actual bearings. The chain-sprocket set up to turn these screws would have worked very well if only the bushings did not have so much friction associated with them. The motor that was used to turn the chain was not powerful enough to overcome the friction associated with the bushings. An alternate actuation idea to make the chord change work could be one of two options. The first is to replace the plastic bushings with bearings. Secondly, the chord change could be actuated with a winch servo just like the span change. If the chord extension would slide along a low friction track a pull-pull system could be implemented to move it.

The sweep change also had an undersized motor associated with it. With the size of the wing and the weight of it, the motor was not able to turn the power screw to rotate the wing. If a transmission of some sort, or a more powerful motor was used, this problem could be overcome. The motors that were purchased for this project had no specifications on their packaging as to how much load they could handle or how much torque was output. So our team had to take a chance on them to see if they would work or not. The only information given on the motors was how much RPM they had “under load”. The load was not even specified. Another problem faced was during a test run before entering the wind tunnel, the sweep motor turned too fast. This swept the wing back very fast until it crashed into its stopping point. This loosened some of the glue in the aluminum anchoring rod, allowing the wing to bend down or up when under load. There was not a huge amount of play in the wing after this incident, but it prevented us from rotating the wing to find the stall angle.

The results from this semester were not all that our team hoped they would be. Our team was only able to have one morph change under load in the wind tunnel. This is a third of our original goal, which was to morph three changes under load. With the results from this semester we are able to make changes for next semester and build a plane that will be able to not only fly, but morph its wings during flight as well.

7.2 Foam Model Testing Conclusions

The experiments done on the models allow drawing some important conclusion about design choices in this project.

- No early separation occurred as predicted by theory. Not a single of the numerous tests have shown any tangible sign of early stall.
- The stall pattern is improved by the chord extension. The modification of the profile induces a smoother transition to the total loss of lift at high angle of attack
- Clear improvement of the lifting capacity of the chord extended profiles was demonstrated. The measurement done on the three profiles used to make this experiment showed a clear increase in lifting coefficient. The tests showed increase in lift of up to 50% from the retracted version.
- Based on Take off criteria the Clark Y profile is clearly the best profile choice tested.

Unfortunately we have been limited in our conclusion by some restrictions. The most important was the failure of the wind tunnel acquisition system. Only the lift coefficient could be analyzed the other coefficient like the drag or pitch coefficient. These coefficients are necessary to explore and optimize the design for flight conditions other than take off/ landing like loiter. Also these values are also necessary for stability and control purposes. But even with these limitations, this experiment has clearly proven that the chord extension was beneficial to the aerodynamic performance of the wing.

7.3 Goals for Next Semester

The main priority of next semester will be for the team to refine the current design and then incorporate it into a fully functional radio controlled model. Due to the difficulties we encountered by trying to morph the sweep, chord and span we would like to focus on only two form changes. We also hope to reduce the overall size of the wing. New design work will need to be done in the fuselage and tail area. We hope that we are able to return to the wind tunnel once the full model has been built to take more data to confirm our aerodynamic predictions. Control surface design has been neglected to this point but is mandatory to construct a working model. The engine we are planning to use is old and still in another aircraft; we need to clean and test it to make sure that it is fully operational. For electrical work we hope to avoid using servo actuated switches and explore the use of PIC controllers or some other substitute.

The final aspect we hope to include is a variable mass that adjusts the center of gravity to account for different morphing conditions. As of now we plan to incorporate a mass that translates

along with the sweep mechanism to counter act the center of gravity as it travels to the rear of the aircraft.

Appendix A:
Test Data for Foam Models

Table A1. Lifting characteristics of the Clark Y

Clark Y							
Retracted				Extended			
α	α*	CL	CL*	α	α*	CL	CL*
-6.0	-2.0	-0.149	-0.149	-6.0	0.0	-0.013	-0.017
-3.9	0.1	0.000	0.000	-3.9	2.1	0.151	0.202
-1.9	2.1	0.137	0.137	-1.9	4.1	0.326	0.435
0.1	4.1	0.294	0.294	0.1	6.1	0.489	0.652
2.0	6.0	0.422	0.422	2.1	8.1	0.634	0.845
4.0	8.0	0.565	0.565	4.1	10.1	0.772	1.029
6.1	10.1	0.700	0.700	6.1	12.1	0.898	1.197
8.1	12.1	0.823	0.823	8.1	14.1	0.912	1.216
10.1	14.1	0.918	0.918	10.1	16.1	0.943	1.258
12.1	16.1	0.996	0.996	12.1	18.1	0.943	1.258
14.1	18.1	0.884	0.884	14.1	20.1	0.839	1.118
16.1	20.1	0.902	0.902	16.1	22.1	0.783	1.044
18.1	22.1	0.867	0.867	18.1	24.1	0.746	0.995
20.1	24.1	0.851	0.851	20.1	26.1	0.773	1.031

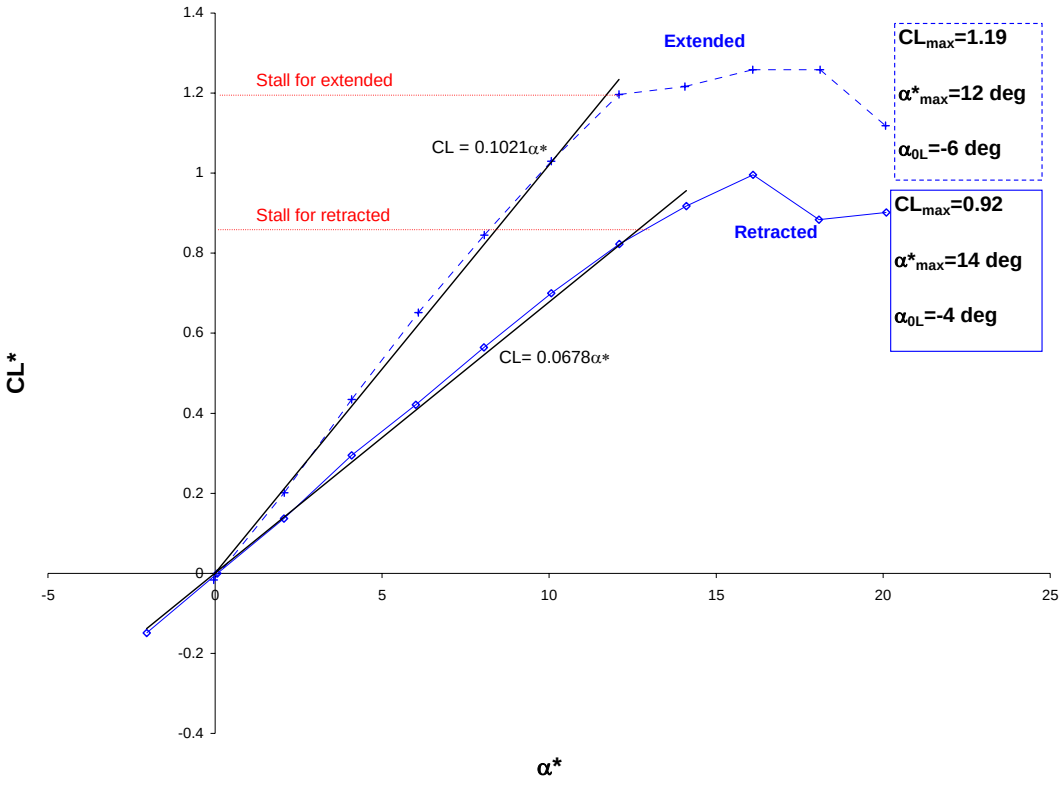

Figure A1. Lifting characteristics of Clark Y original & modified

Table A2. Lifting characteristics of the Selig 8036

Selig							
Retracted				Extended			
α	α*	CL	CL*	α	α*	CL	CL*
-7.7	-5.6	-0.379	-0.379	-7.5	-4.8	-0.411	-0.548
-5.6	-3.5	-0.255	-0.255	-5.4	-2.7	-0.231	-0.308
-3.5	-1.4	-0.102	-0.102	-3.4	-0.7	-0.062	-0.082
-1.5	0.6	0.035	0.035	-1.4	1.3	0.100	0.133
0.5	2.6	0.160	0.160	0.7	3.4	0.250	0.333
2.5	4.6	0.292	0.292	2.6	5.3	0.400	0.534
4.5	6.6	0.413	0.413	4.6	7.3	0.540	0.720
6.5	8.6	0.547	0.547	6.6	9.3	0.682	0.910
8.5	10.6	0.653	0.653	8.7	11.4	0.792	1.057
10.5	12.6	0.737	0.737	10.7	13.4	0.837	1.116
12.5	14.6	0.800	0.800	12.6	15.3	0.847	1.130
14.5	16.6	0.795	0.795	14.6	17.3	0.857	1.143
16.5	18.6	0.716	0.716	16.7	19.4	0.835	1.113
18.5	20.6	0.741	0.741	18.6	21.3	0.814	1.085

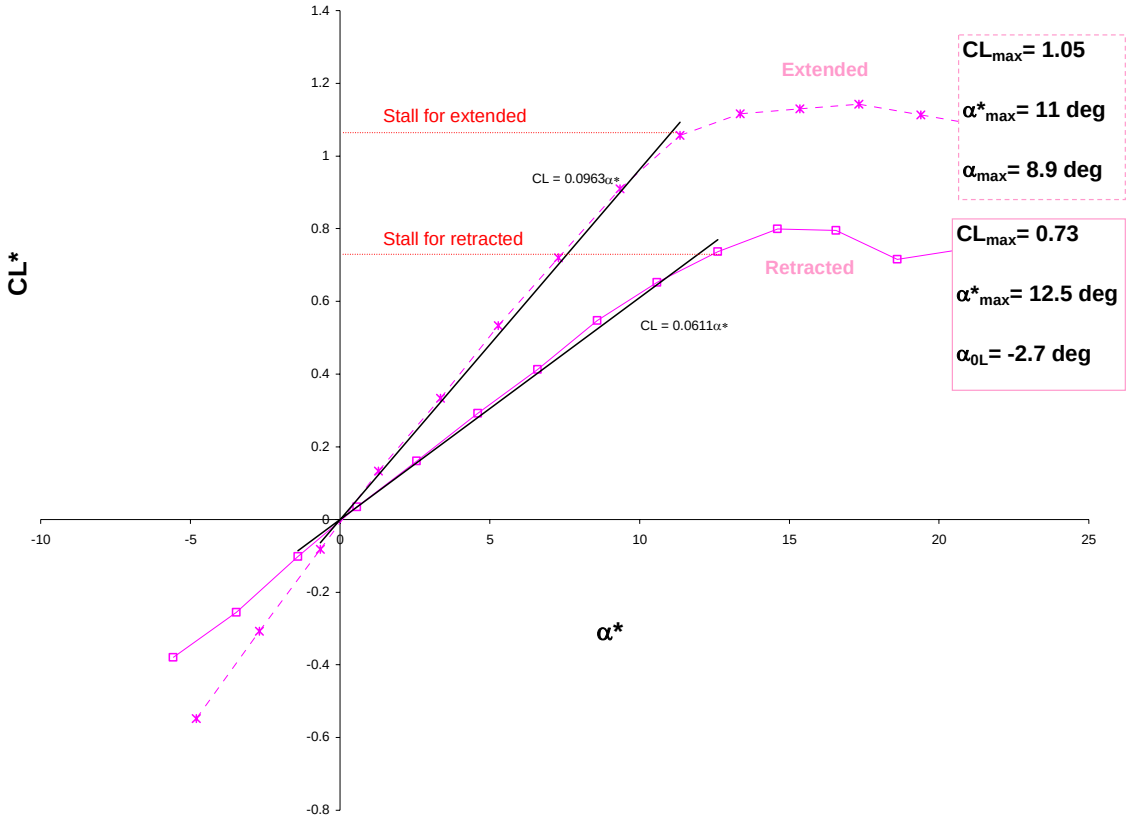

Figure A2. Lifting characteristics of Selig 8036 original & modified

Table A3. Lifting characteristics of the Eppler 168

Eppler							
Retracted				Extended			
α	α*	CL	CL*	α	α*	CL	CL*
-4.1	-2.1	-0.179	-0.179	-6.4	-2.6	-0.195	-0.260
-2.0	0.0	0.002	0.002	-4.2	-0.4	-0.031	-0.041
0.1	2.1	0.179	0.179	-2.2	1.6	0.121	0.162
2.0	4.0	0.339	0.339	-0.3	3.5	0.277	0.369
4.1	6.1	0.497	0.497	1.7	5.5	0.419	0.559
6.1	8.1	0.608	0.608	3.7	7.5	0.548	0.731
8.1	10.1	0.655	0.655	5.8	9.6	0.643	0.858
10.1	12.1	0.634	0.634	7.8	11.6	0.696	0.928
12.1	14.1	0.678	0.678	9.7	13.5	0.691	0.921
14.1	16.1	0.462	0.462	11.8	15.6	0.670	0.894
16.1	18.1	0.441	0.441	13.8	17.6	0.664	0.885
18.1	20.1	0.468	0.468	15.8	19.6	0.598	0.798
20.1	22.1	0.419	0.419	17.8	21.6	0.590	0.787
22.1	24.1	0.475	0.475	19.8	23.6	0.607	0.810

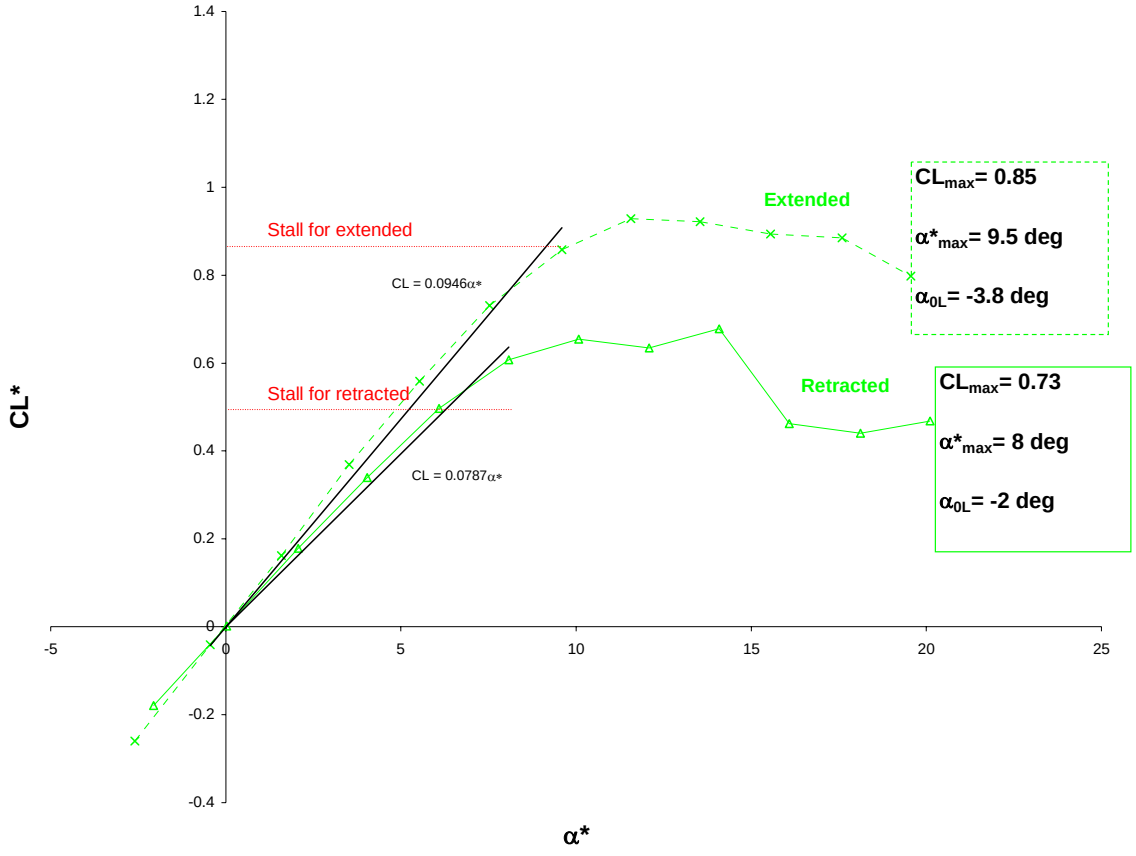

Figure A4. Lifting characteristics of Eppler 168 original & modified

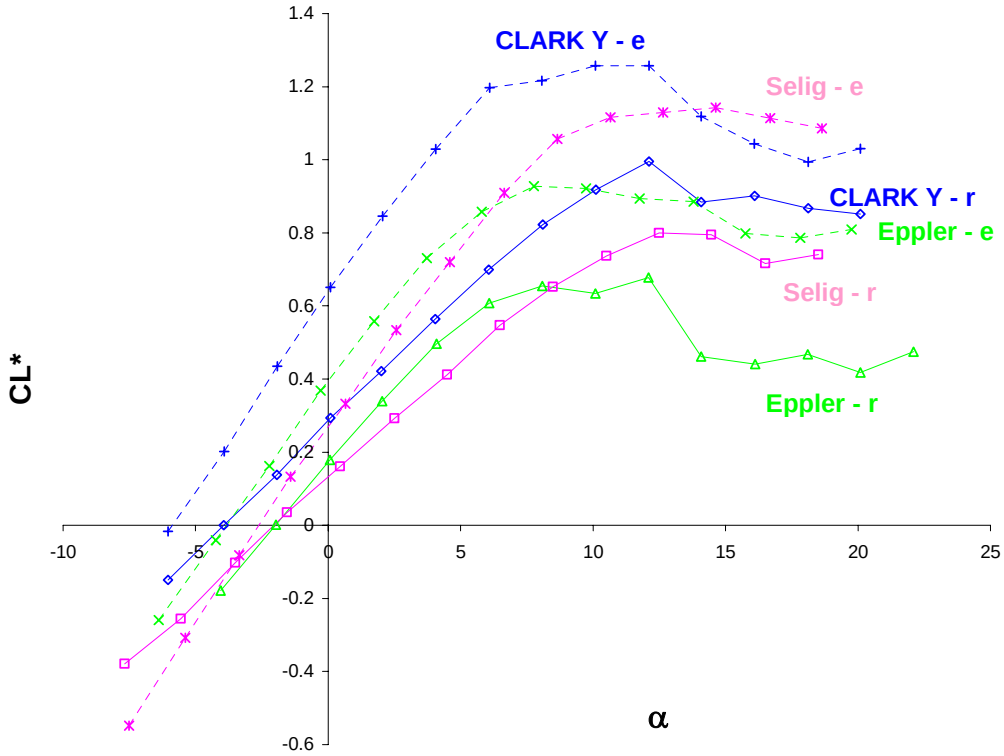

Figure A5. Comparison plot with CL* vs α

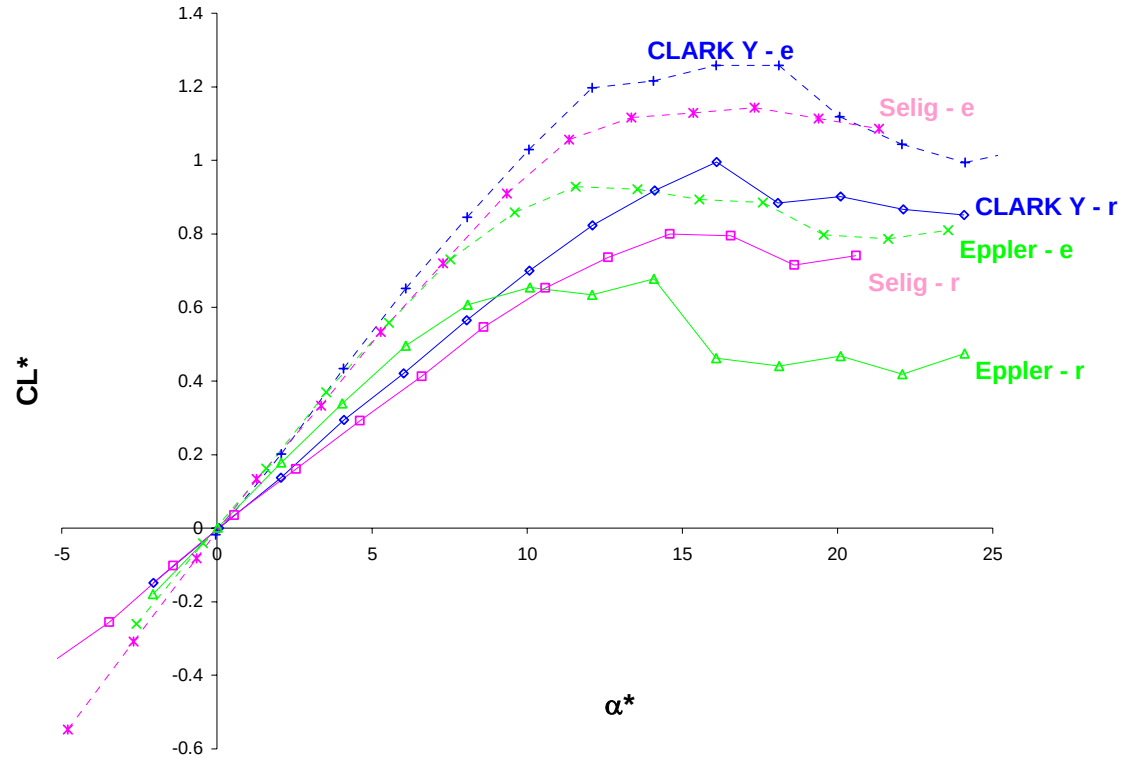

Figure A6. Comparison plot with CL* vs $\alpha*$

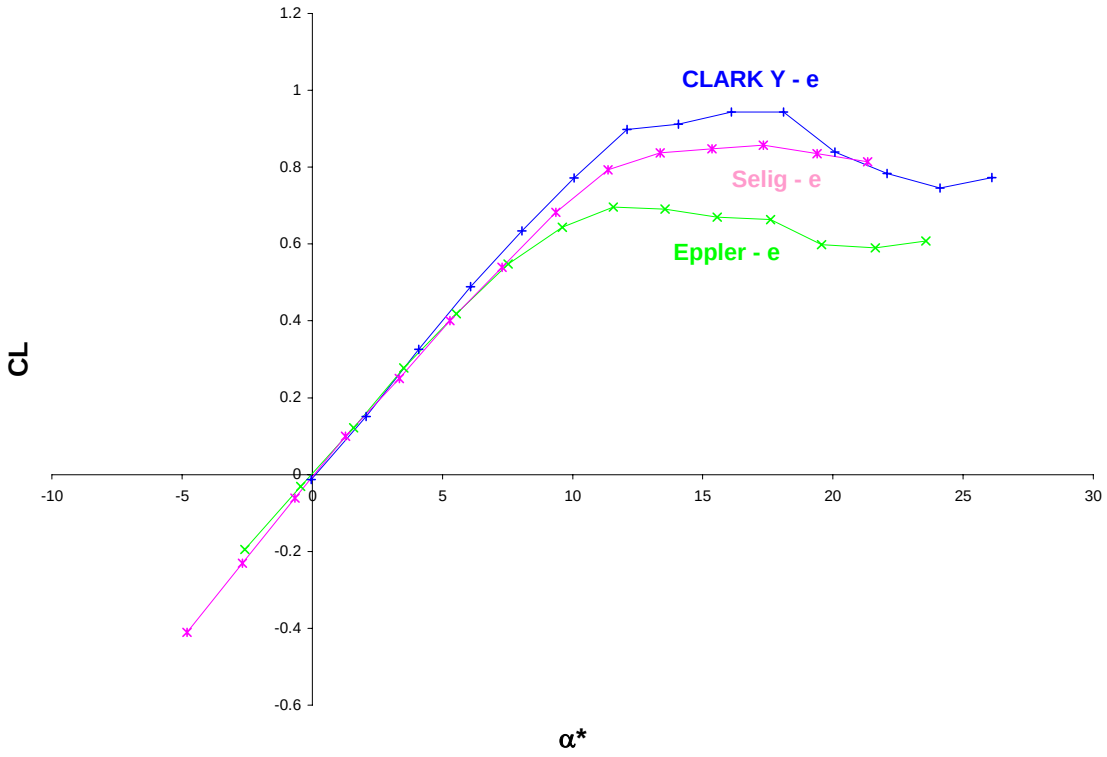

Figure A7. Lift Coefficient characteristics of modified wing profiles

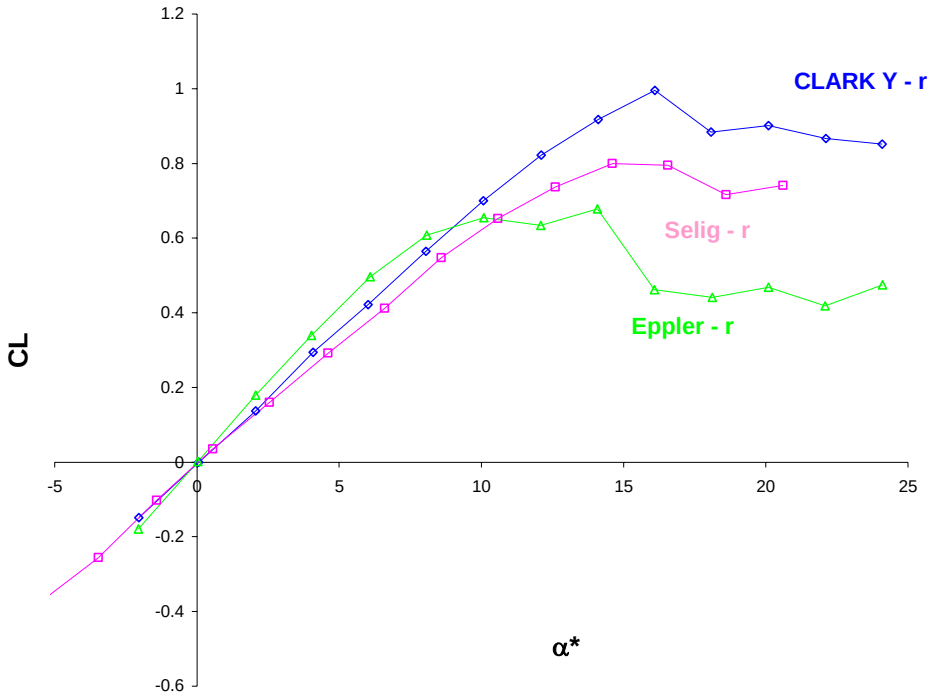

FigureA8. Lift Coefficient characteristics of original wing profiles

TableA5. Lifting characteristics of the profile options

	CLARK Y		Selig		Eppler	
	r	e	r	e	r	e
CL^*_{α}	0.0678	0.0678	0.0661	0.0963	0.083	0.095
CL^*_{max}	0.92	1.19	0.73	1.05	0.6	0.85
α_{0L} [°]	-4	-6	-2.1	-2.7	-2	-3.8
$\Delta\alpha_{max}$ [°]	14	12	12.5	11	8	9.5

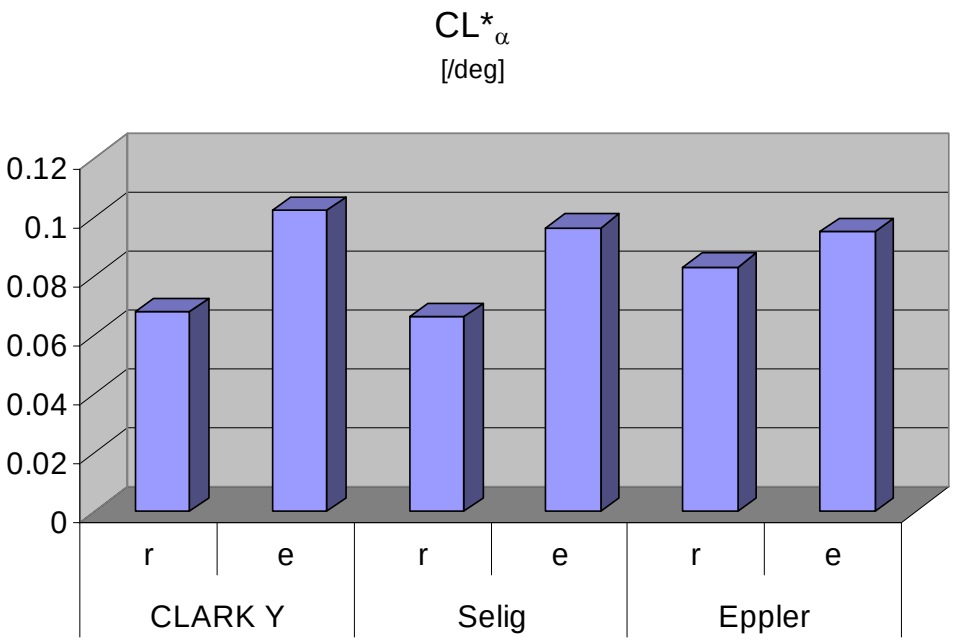

Figure A9. Comparison of the lift curve slopes (r-retracted/e-extended)

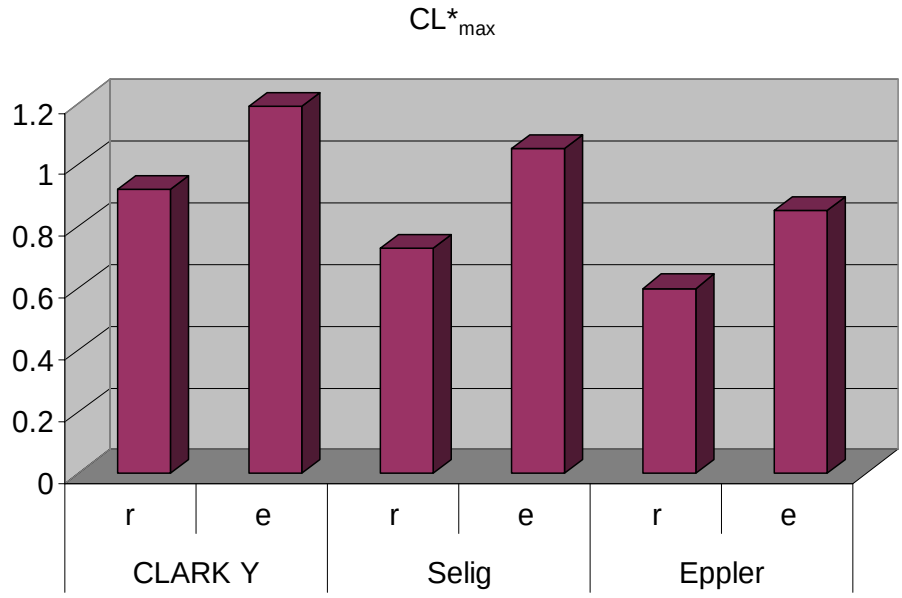

Figure A10. Comparison of the maximum lift available (r-retracted/e-extended)

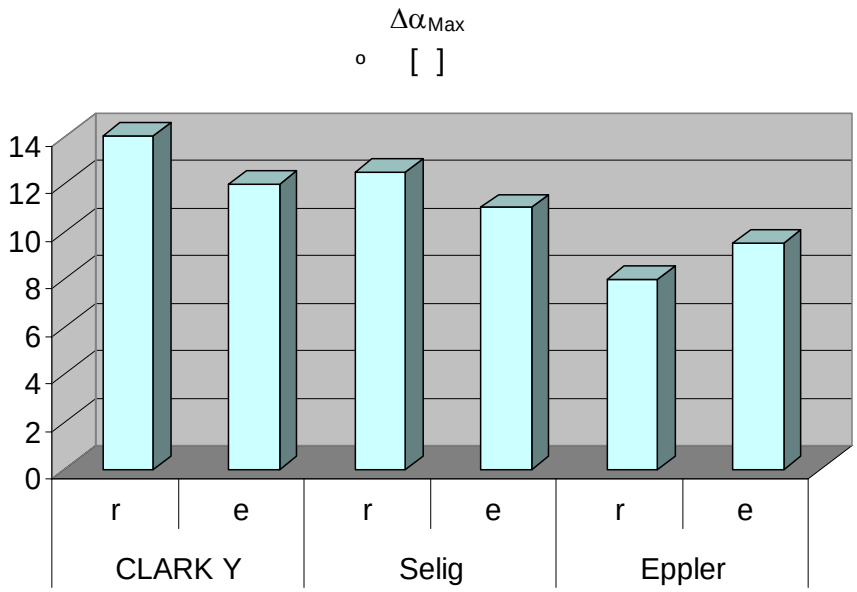

Figure A11. Comparison of the angle of attack range available

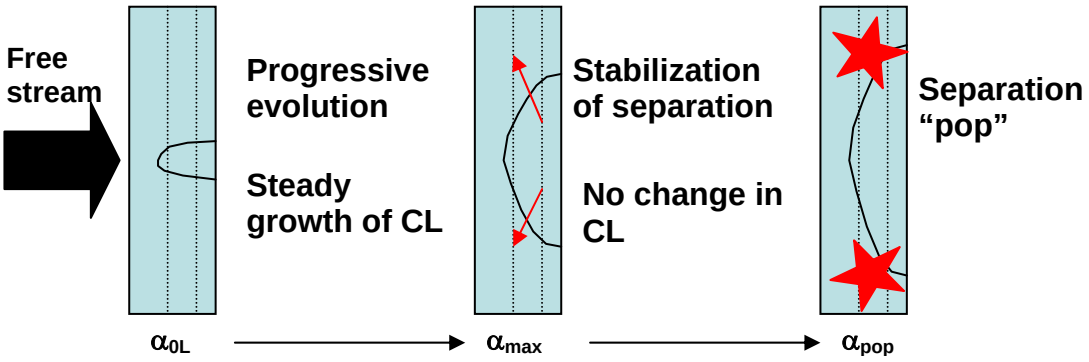

Figure A12. Description of flow separation as seen during the tufts visualization

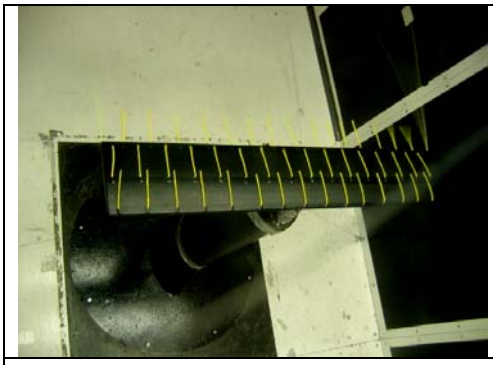

α =4°

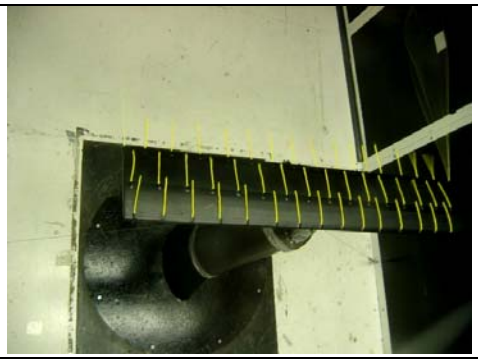

α =6°

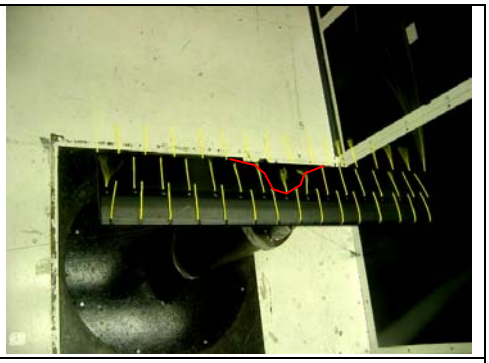

α =8°

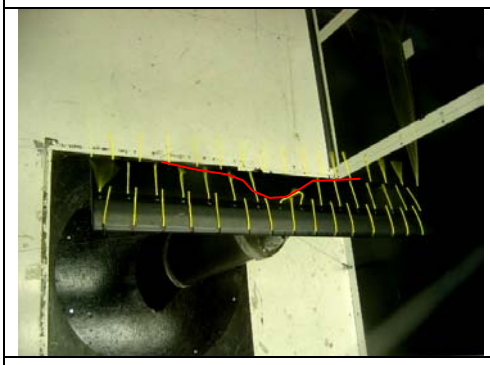

α =10°

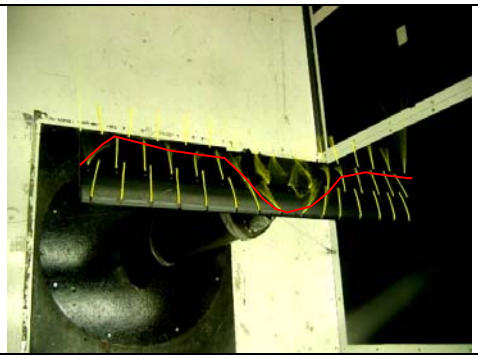

α =12°

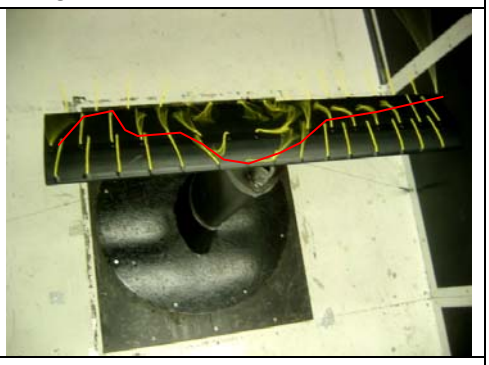

α =14°

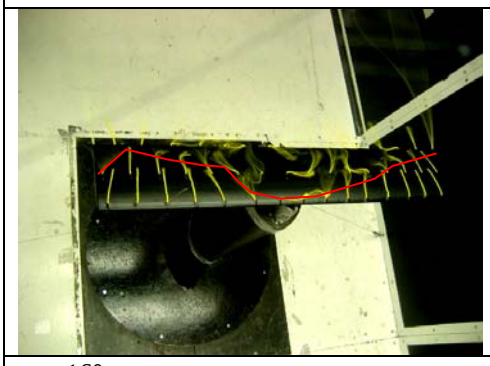

α =16°

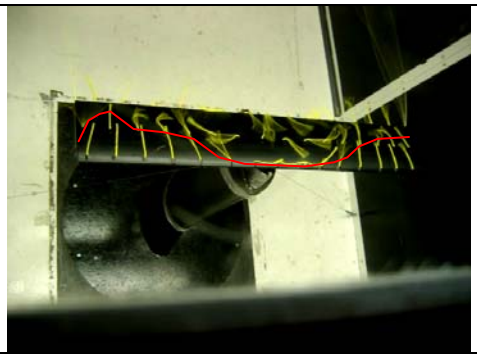

α =20°

Figure A13. Evolution of flow separation on original Clark Y see

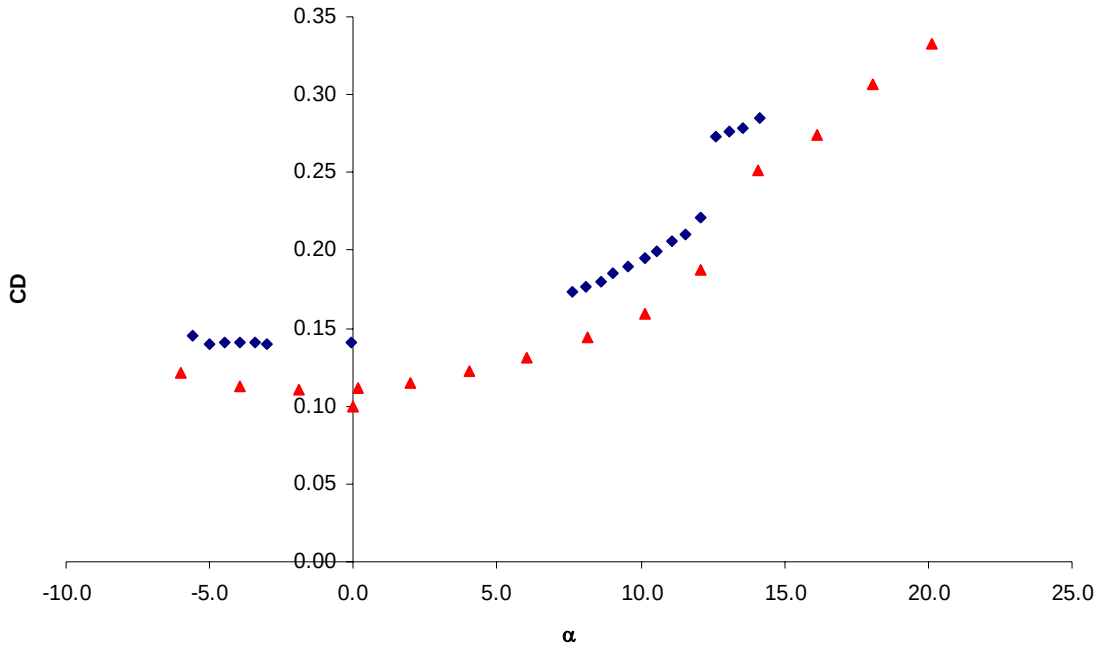

Figure A14. Non repeatability of drag measurements (Data taken from Clark Y-r)

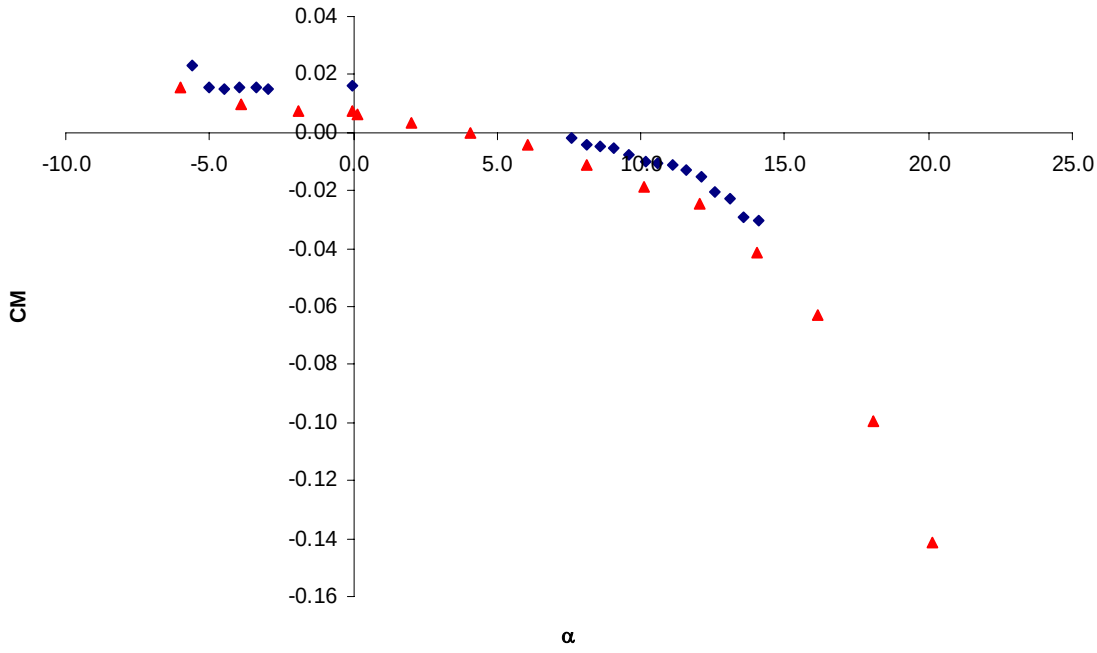

Figure A16. Non repeatability of pitching moment measurements (Data taken from Clark Y-r)

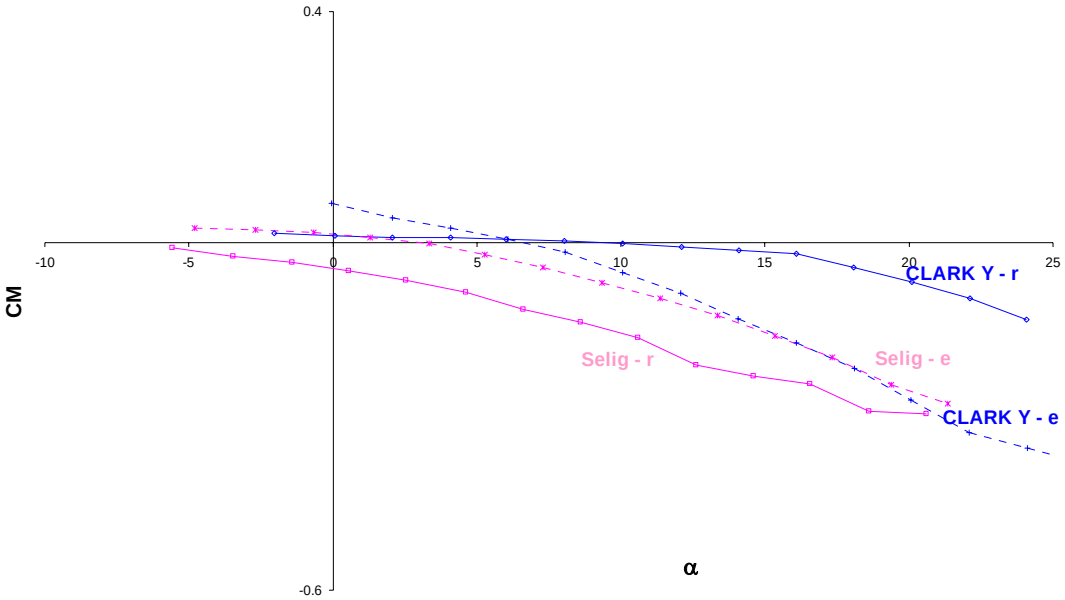

Figure A17. Qualitative representation of the models pitching moment

Appendix B:
Supplemental Drawings

References

"Century of Flight," (Pilot Friend, 2004) *http://www.pilotfriend.com/century-of-flight/index.htm*, December 10, 2004.

"F-14 Tomcat," (Military Analysis Network, 2000) *http://www.fas.org/man/dod-101/sys/ac/f-14.htm*, December 10, 2004.

Marks, Paul,"The Next 100 Years of Flight-Part 2," (New Scientist, 2003) *http://www.newscientist.com/article.ns?id=dn4484* December 10, 2004.

Mason, William, "AOE 3054 lab manual, experiment 7," (Blacksburg, VA: AOE Department, 2003),

AOE 3054: Lab Manual